Chapter 5
Investigation of Wear Induced Layer in Al-Al_3Ti Functionally Graded Material

5.1. Introduction

In chapter 4, wear anisotropy of Al-Al_3Zr FGMs fabricated by centrifugal solid-particle method (CSPM) has been investigated. A wear induced layer containing supersaturated Al-Zr solid-solution has been observed and it was briefly explained. In this chapter, more detailed discussion about the formation mechanism of this layer, its thickness and its evidence will be presented. In addition, the optimum wear test parameters required to form such layer are also discussed. As FGMs, Al-Al_3Ti FGMs fabricated by CSPM method has been used for the investigation.

According to the reported compositional gradient obtained in Al-Al_3Ti FGMs [1-4], the outer surface of the fabricated Al-Al_3Ti FGMs has always higher density of Al_3Ti particles and hence higher wear resistance compared to the inner parts. Watanabe *et al.* [5] have investigated the microstructure near the worn surface during the wear test of Al-Al_3Ti FGMs. They have observed that a wear induced layer of 100 μm thickness is formed just below the worn surface. Furthermore, when subjected to heat treatment, the wear induced layer is decomposed into Al and small Al_3Ti particles [6, 7].

Recently, Sato *et al.* [8] have reported that the wear induced layer consists of nano-crystalline (NC) solid solution matrix of Ti in Al, fine fibrous Al_3Ti particles and a partly amorphized phase. However, the effect of wear test conditions on the formation of such layer has not been yet investigated. Some theoretical and experimental discussion about the wear induced layer in wear tested Al-Al_3Ti FGM samples is, therefore, given in this chapter.

5.2. Experiments

5.2.1. Preparation of Al-Al_3Ti FGM rings

The horizontal type centrifugal casting machine shown in Fig. 4.1 has been used for the current experiments. A commercial Al-5 mass% Ti alloy containing Al_3Ti platelet particles was used as master alloy. Since the relative atomic masses of Al and Ti are 26.98 and 47.9, respectively, the theoretical volume fraction of Al_3Ti particles is calculated to be 11 vol.%. The processing temperature was 900°C, which is significantly lower than the liquidus temperature of the master alloy (see Fig. 1.1). On this way, the Al_3Ti particles will remain solid in the liquid Al matrix during the mold rotation as explained about CSPM in section 1.2.2. The melt was then poured into a 650°C preheated cylindrical mold. A centrifugal force magnitude of G=80 was applied. The fabricated FGMs have a dimension of 90 mm outer diameter and 30 mm wall thickness. The samples microstructure on the ring three planes was observed by OM and SEM. The volume fraction of Al_3Ti particles was measured by evaluating the area fraction of Al_3Ti on plane OP2 (observation plane) with 0.2 mm interval.

5.2.2. Wear test of Al-Al_3Ti FGM samples

Wear tests of the fabricated samples were carried out using a block-on-disc-type wear machine under rotary movement. The counter disc was S45 C steel with 80 mm diameter and 190 Hv hardness. Before the wear test, the counter disc was mechanically polished using SiC paper. The wear test was performed with an initial stress of 0.5 MPa and 1 m/s and 2 m/s sliding speeds. The sliding distances ranged between 1 to 4 km. Wear tests were performed on plane OP3, which coincides with the outer surface of the FGM ring as illustrated in Fig. 5.1. As a result, the contact between the FGMs samples and the counter disc occurred in a condensed region of Al_3Ti particles. The specimen cutting direction and their dimensions are shown in Fig. 5.1. After the wear test, the microstructure of the worn samples was studied on the plane parallel to the sliding direction, named OP2 in Fig.5.1. The OM and SEM were used for microstructural observation. The distribution of Ti and Al in the sub-worn surface layer and the following layers were observed by energy-dispersive X-ray spectroscopy (EDS).

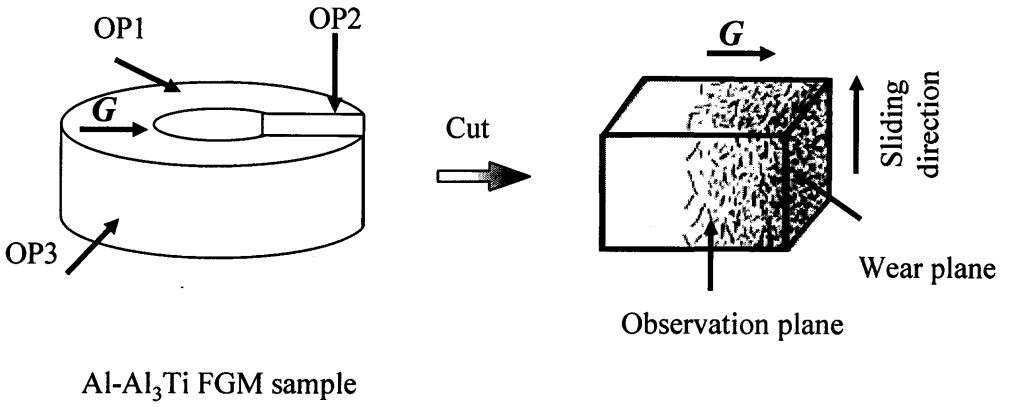

Fig. 5.1. Al_3Ti FGM sample and wear test sample cutting direction.

5.3. Results and discussion

5.3.1. Original microstructure of Al-Al_3Ti FGMs

OM photographs of Figs. 5.2 (a) and (b) are showing the microstructure of the particles rich area of Al-Al_3Ti FGM sample on the side plane and the wear plane respectively. It is clear from Figs. 5.2 (a) and (b) that the Al_3Ti platelet particles are closely oriented normal to the centrifugal force. The Al matrix in these micrographs has equiaxed grains on the three planes. The volume fraction distribution of Al_3Ti particles from the wear surface to the inner of the FGM ring is shown in Fig. 5.3. The particles volume fraction remarkably decreases towards the inner surface of the ring. The outer ring surface (wear surface) showed around 30% then this percent gradually decreased upon increasing the distance from worn surface. The Al_3Ti platelet particles very close to the outer ring surface showed a tendency to align normal to the centrifugal force as clear from Fig. 5.4. The Hermans' orientation parameter in this figure is calculated from eq. (2-1) in section 2.3.1. Furthermore, the hardness distribution gradient presented a similar trend to that of particles volume fraction and particles orientation. Figure

5.5 shows the hardness distribution in the fabricated FGM rings from the outer to the inner of the Al_3Ti FGMs sample.

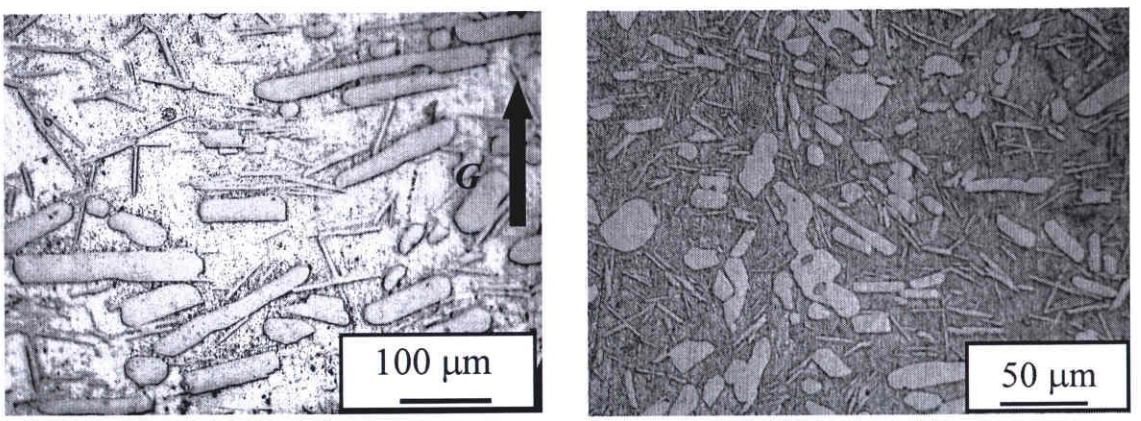

OP2 **OP3**

Fig. 5.2. Microstructure of Al_3Ti FGM sample on planes OP2 and OP3, presented in Fig.5.1.

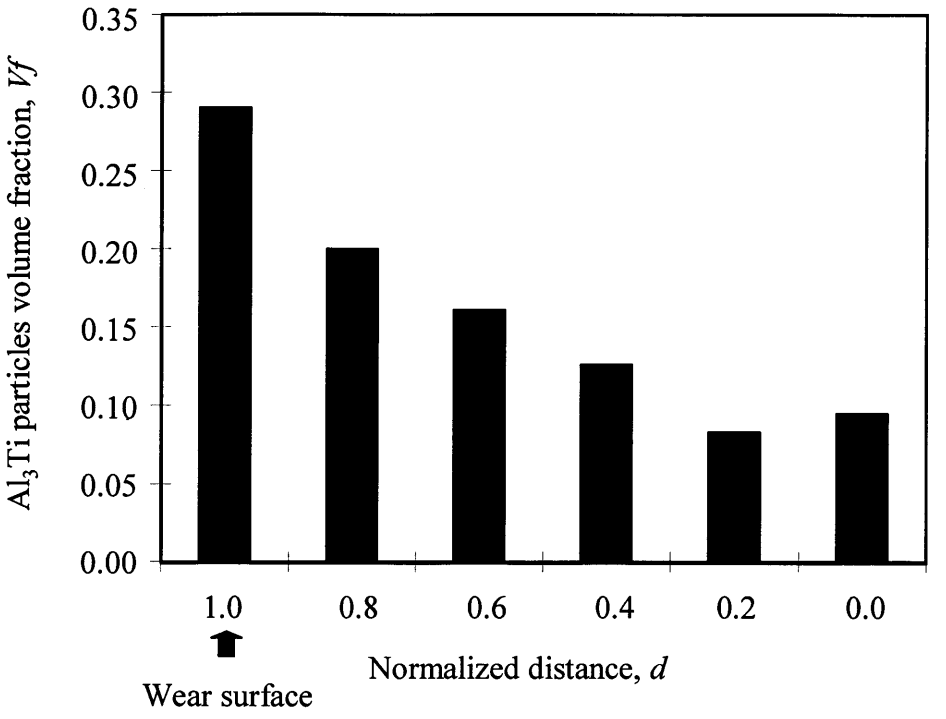

Fig.5.3. Volume fraction distribution of Al_3Ti along the FGMs ring thickness.

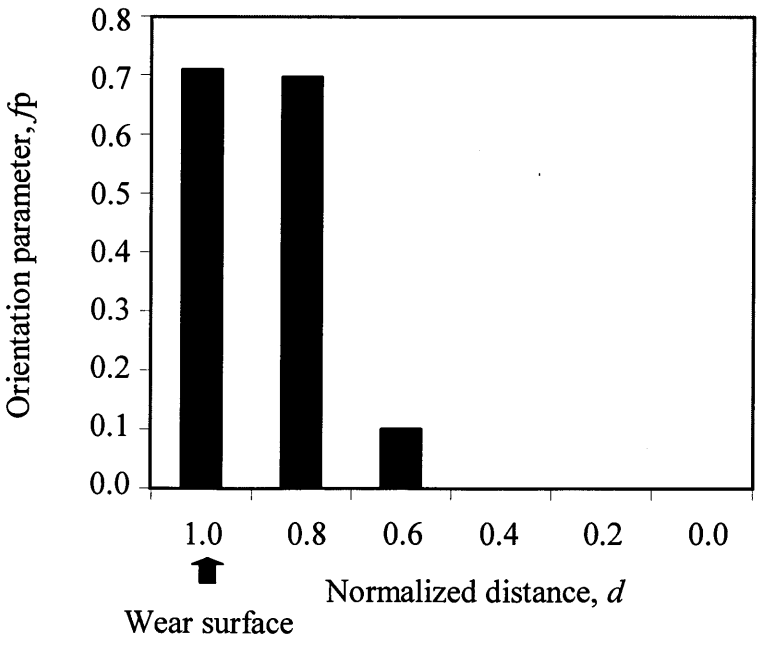

Fig.5.4. Orientation distribution of Al_3Ti platelet particles along the sample thickness.

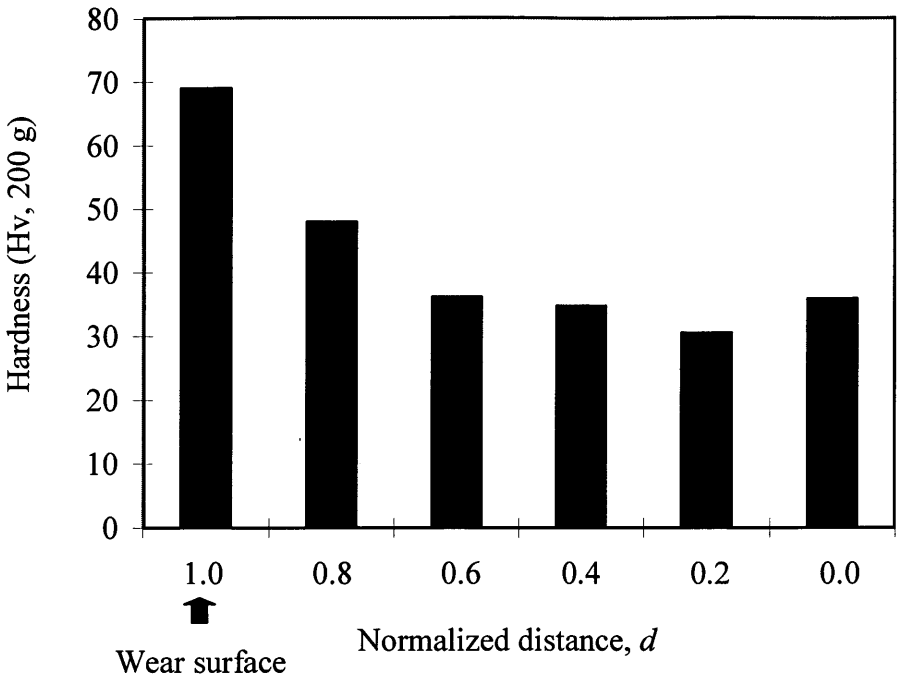

Fig.5.5. Hardness distribution along Al-Al_3Ti FGMs ring thickness.

5.3.2. Wear resistance and wear induced microstructure of Al-Al_3Ti FGM

The wear resistance of Al-Al_3Ti FGMs showed a continuous decreasing trend with increasing the sliding speed. Fig. 5.6 shows the relationship between the sliding distance, *SD*, and the weight loss of Al-Al_3Ti FGM samples tested at constant speed of 1 m/s. The microstructure of the side surface of the FGMs tested on different sliding distance conditions is shown in Fig. 5. 7. It is observed that the samples microstructure at *SD* of 1 km and 2 km is almost similar to the initial microstructure of Al-Al_3Ti FGMs on plane OP2, Fig. 5.2. However, the sub-worn surface microstructure of 3 km tested samples showed different microstructure. The layer just below the worn surface, named as wear induced layer [5-7], could be identified when the *SD* increased to 3 km. On the other hand, increasing the wear test speed to 2 m/s caused severe deformation of the sub-worn surface and the wear induced structure could be observed even at *SD* of 1 km *SD*, as shown in Fig. 5.8. Though the quantitative analysis was not carried out, it was found that the thickness of this layer increased when the wear test was

performed at higher *SD* as observed from SEM micrographs. Performing the test at *SD* over 3 km resulted in absence of this wear induced structure. This because most of the intermetallics reach area was already removed under the action of wear.

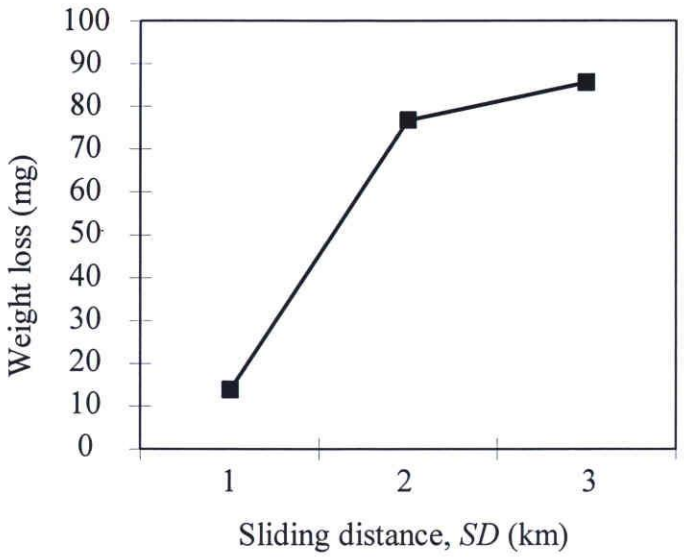

Fig.5.6. Weight loss of Al-Al_3Ti FGMs at different sliding speeds.

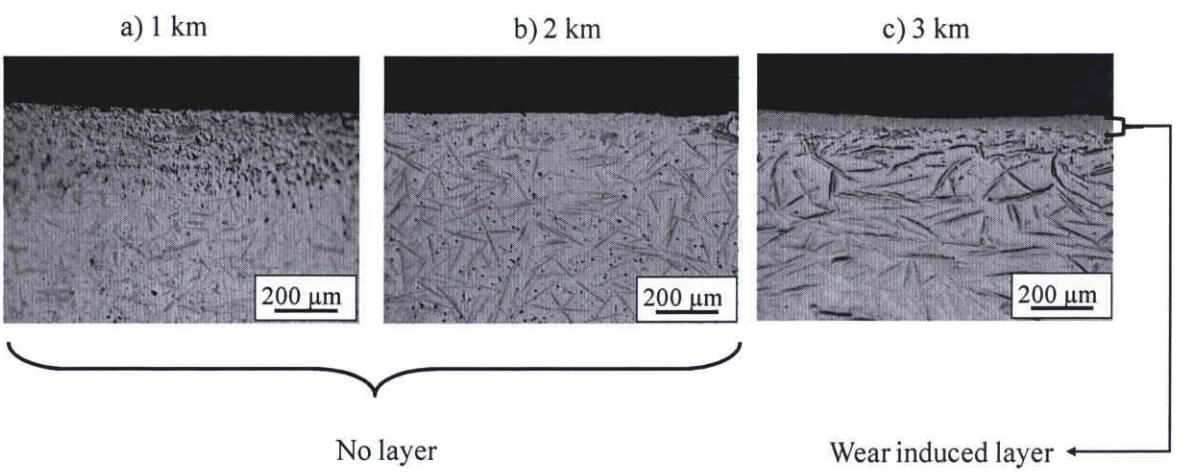

Fig.5.7. OM photographs showing the sub-worn surface microstructures of Al-Al_3Ti FGM at a speed of 1 m/s and different sliding distances.

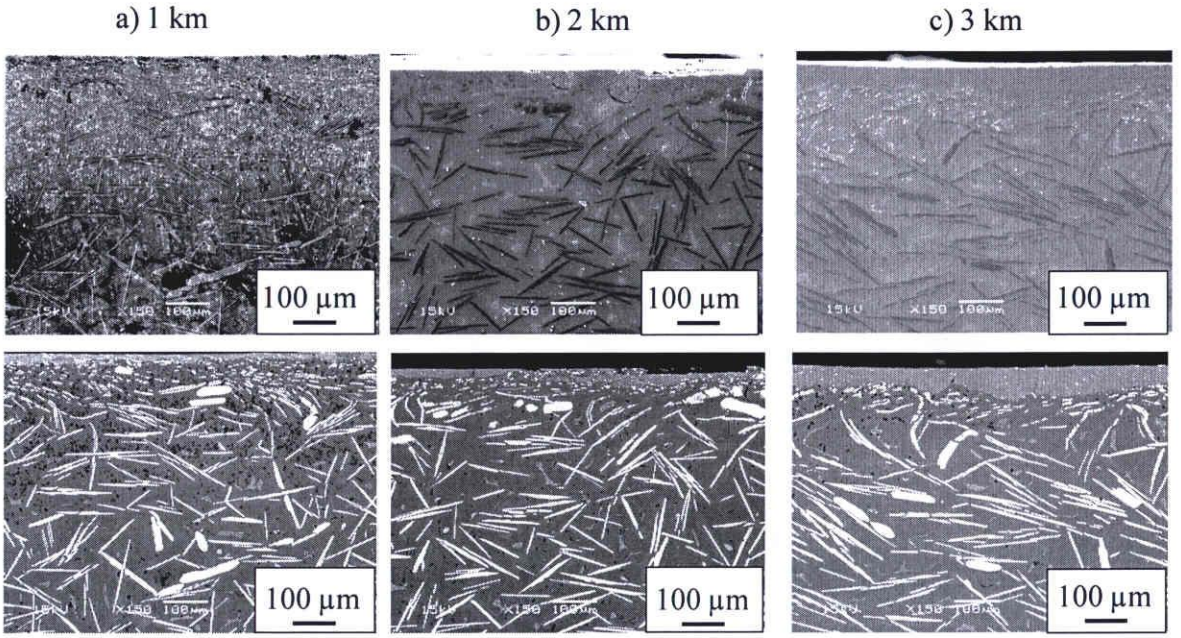

Fig.5.8. SEM micrographs and compositional images of the sub-worn surface of Al-Al_3Ti FGM at a speed of 2 m/s and different sliding distances.

5.3.3. Investigation of wear induced layer and its formation mechanism

The wear induced layer observed after the wear test of Al-Al_3Ti FGM was studied using EDS. Since the samples tested under higher speed, 2 m/s, showed more significant changes in their microstructure after the wear test, the wear induced layer in these sample was studied at different *SD*. Figures 5.9 to 5.11 present the Ti and Al maps obtained from EDS analysis of the sub-worn surface layers. Two observation areas were chosen to further confirm the obtained result. Here it is worth mentioning that increasing the test speed and *SD* increased the thickness of the wear induced layer and increased the free Ti in the matrix accordingly. The Ti distribution in the wear induced layer and the following layers is shown in Figs. 5.12 (a) and (b) respectively. According to Fig. 5.12, some free Ti in the wear-induced layer was dispersed uniformly in the Al matrix and not condensed in Al_3Ti particles. The composition of Ti in the

supersaturated layer shown in Fig. 5.11 as an example, was analyzed to be roughly 7 mass % and this percent decreased in the following layers. Since the solubility of Ti in Al is 1.24 % at 665°C [9], the Ti concentration in the wear induced layer exceeds however this solubility limit. This further confirms the formation of the Al-Ti supersaturated solid solution without the presence of Al_3Tiparticle.

The wear induced layer was reported by Sato *et al.* [8] to consist of NC solid-solution matrix of Ti in Al, fine fibrous Al_3Ti particles and a partly amorphized phase [10]. The grain sized of the observed NC matrix was about 16 nm [8]. The sequence of the process was explained as follows; first: when the onset of the wear test reached, the shear deformation occurs on the surface followed by work hardening of Al matrix locally. Secondly; this deformation then induces the fragmentation of the Al_3Ti particles. Therefore, the platelet particles are changed to granular shaped particles dispersed in elongated Al grains. Thirdly; as the shear deformation proceeds further, the particles are heavily deformed and become fibrous particles. At the same time, the Al grains are refined and the Al matrix dissolves some Al_3Ti particles. Finally, the wear induced layer consists of an NC-grained supersaturated Al-Ti solid solution, finely dispersed Al_3Ti fibrous particles and a partly amorphized phase on the worn surface [8].

In the scope of the reported data [8] and the current results, formation of the wear induced layer with NC structure can occur only under certain deformation conditions. Therefore, such layer could not been observed in some samples of the current Al-Al_3Ti FGMs. Furthermore, this layer was not formed when the Al-Al_3Ti alloy samples were deformed by ECAP. Since this layer has NC structure, the shear strain required to form such NC grains must be achieved to obtain such layer. The relationship between the effective shear strain required to form the NC structure and the thickness of the sheared grain (5-1) was reported earlier [11].

$$\bar{\delta} = \left(\frac{\frac{D^2}{c^2} - 1}{3} \right)^{\frac{1}{2}} \approx \frac{D}{c\sqrt{3}} \quad (D >> c). \qquad (5\text{-}1)$$

Where D is the grain diameter, δ is the effective shear strain and c is the thickness of the sheared grain. Sato *et al* [8] estimated the shear strain required to form the wear induced layer with NC structure for Al-Al_3Ti FGMs to be 90. Concluding, the formation of such supersaturated layer occurred in the current experiments due to the high shear strain applied to the outer surface of the FGMs ring, which contains a large number of Al_3Ti particles. On the other side, the Al_3Ti particles in case of ECAPed samples are distributed in the sample. In addition, the shear strain provided by ECAP causes severe fragmentation of the particles, thus free Ti could be observed in the matrix but the wear induced layer containing the NC structure couldn't be observed due to the continuous distribution of the particles in the ECAPed sample.

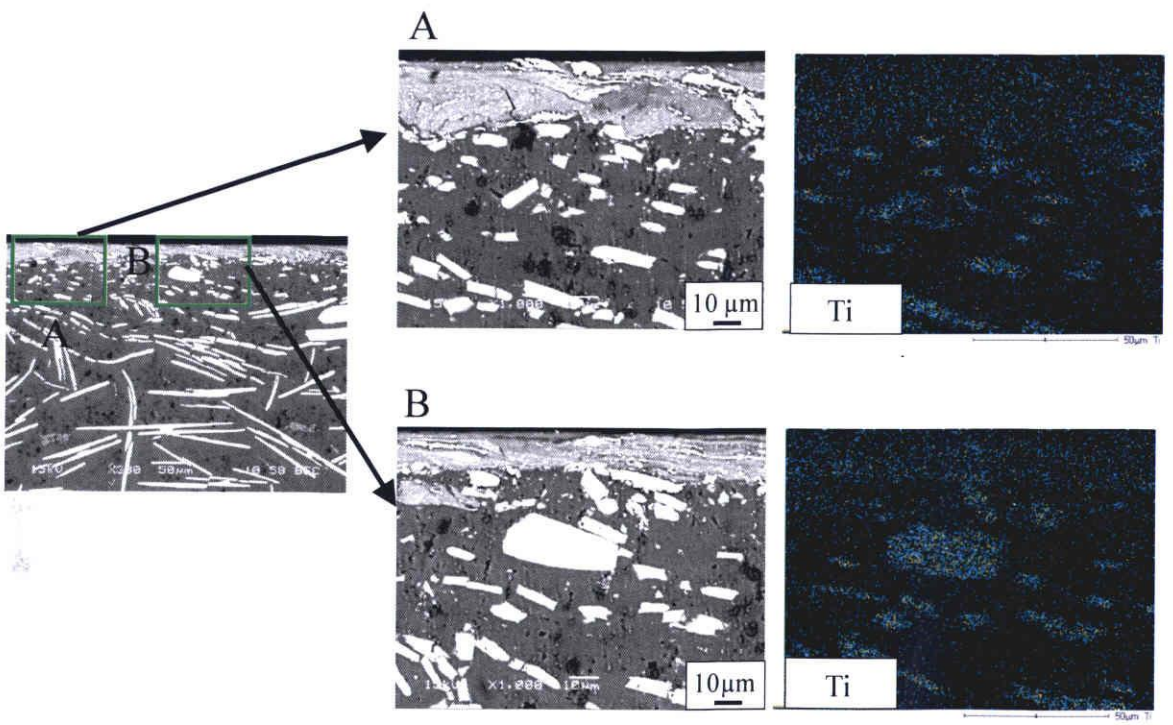

Fig. 5.9. Compositional images and elemental maps of the sub-worn surface layer of Al-Al_3Ti FGM samples tested at 2 m/s, *SD* of 1 km.

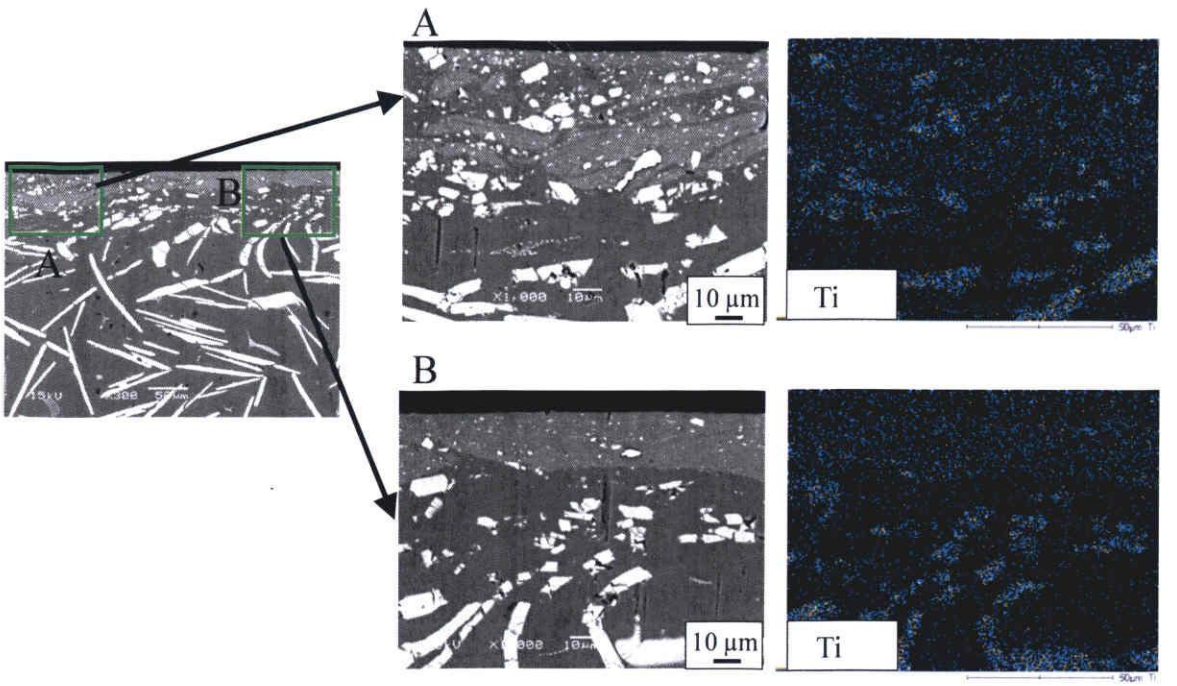

Fig. 5.10. Compositional images and elemental maps of the sub-worn surface layer of Al-Al_3Ti FGM samples tested at 2 m/s, *SD* of 2 km.

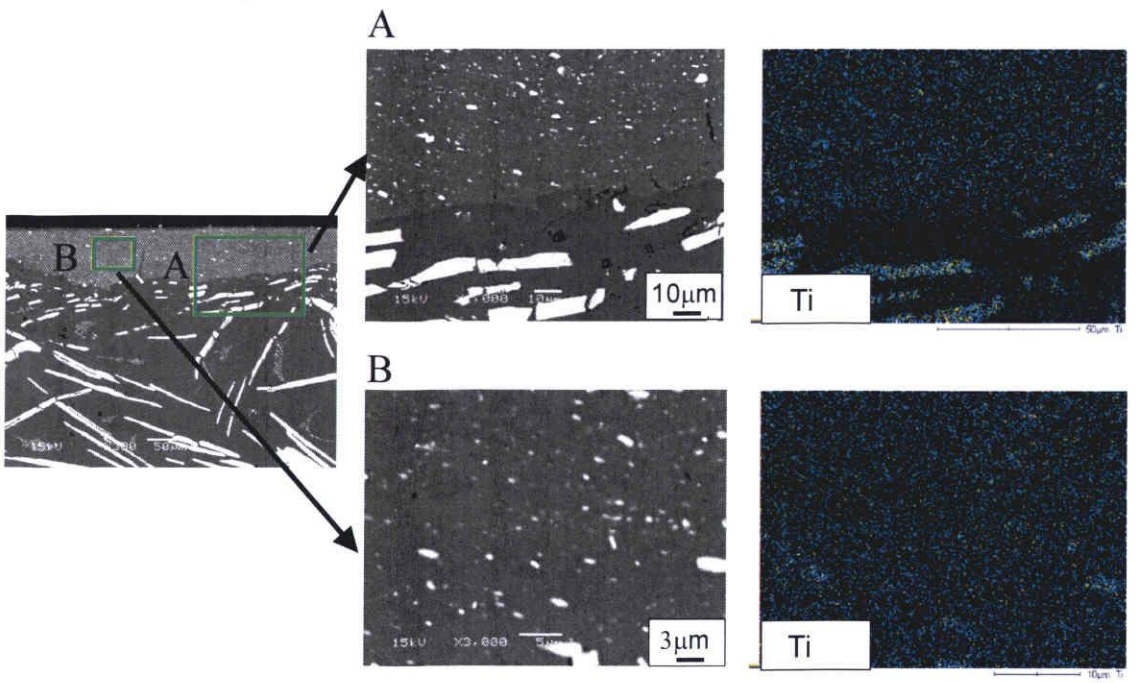

Fig. 5.11. Compositional images and elemental maps of the sub-worn surface layer of Al-Al_3Ti FGM samples tested at 2 m/s, *SD* of 3 km.

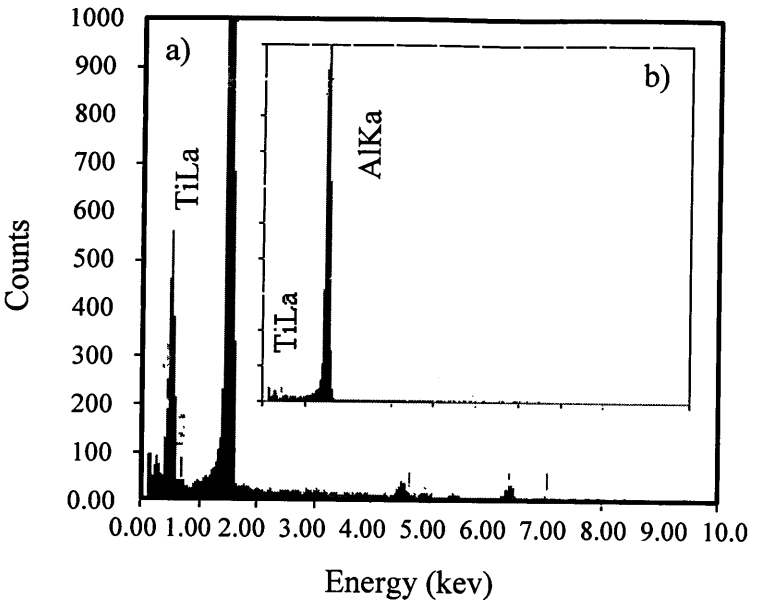

Fig.5.12. Distribution of Ti in a) wear induced layer and b) the following layer of the samples shown in Fig. 5.11.

5.4. Conclusions

In this chapter, effect of wear test conditions on the formation of wear induced layer in Al-Al_3Ti FGMs has been discussed. The presence of such layer in the current FGM samples depends on some experimental variables as sliding speed and sliding distance. At high sliding speed and/or high sliding distance, a severe shear strain can be achieved and thus this layer can be observed. The wear induced layer as observed in the current experiments, includes Al-Ti super saturated solid solution with free Ti particles in addition to some very fine Al_3Ti fibrous particles.

References:

[1] Watanabe Y, Yamanaka N, Fukui Y. Z. Metallkd., 88 (1997) 717.

[2] Watanabe Y, Yamanaka N, Fukui Y. Metall. Mater. Trans. A, 30A (1999) 3253.

[3] Watanabe Y, Eryu H, Matsuura K. Acta Mater., 49 (2001) 775.

[4] Sequeira P.D, Watanabe Y, Eryu H, Yamamoto T, Matsuura K. J. Eng. Mater. Tech. Trans. ASME 129 (2007) 304.

[5] Watanabe Y, Yamanaka N, Fukui Y, Metall. Mater.Trans. A, 30A (1999) 3253.

[6] Yokoyama K, Watanabe Y. Trans. Mater. Res. Soc. Jpn., 26 (2001) 303.

[7] Watanabe Y, Yokoyama K, Hosoda H. Mater. Sci. Forum, 45 (2002) 1467.

[8] Sato H, Murase T, Fujii T, Onaka S, Watanabe Y, Kato M. Acta Mater., 56 (2008) 4549.

[9] Massalki T.B, Murry J.L, Bennet L.H, Baker H. Binary Alloy Phase Diagrams. Metals Park: ASM; 1986

[10] Li X.Y, Tandon K.N. Acta Mater., 44 (1996) 361.

[11] Dautzenberg J.H, Zatt J.H. Wear, 23 (1973) 9.

Chapter 6
Microstructure and Mechanical Properties of Al-Al_3Ti FGMs Fabricated by Centrifugal *in-situ* and Solid-Particle Methods

6.1. Introduction

Fabrication of functionally graded materials (FGMs) by centrifugal *in-situ* method (CISM) and centrifugal solid-particle method (CSPM) [1-6] were explained in section 1.2.2 and a schematic illustration of the two methods was presented in Fig. 1.6. In previous studies, it has been reported that CISM-FGMs have a slower gradient and smaller particles size compared to CSPM-FGMs [4, 8]. However, the differences of mechanical properties between CISM and CSPM have not been investigated. Generally, particle distribution in a composite determines its mechanical property [9, 10]. If the centrifugal method (CM)-FGMs are practically applied, the dependency of the mechanical properties on the processing method should be clear.

In this study, microstructure and mechanical properties of Al-Al_3Ti FGMs fabricated by the CISM and CSPM were investigated. As mechanical properties, wear test and hardness test were carried out. Based on the obtained results, the differences of mechanical properties between CISM-FGMs and CSPM-FGMs were discussed.

6.2. Experimental procedure

6.2.1. Fabrication of FGMs

Al-Al_3Ti FGMs were produced using a commercial Al-5 mass%Ti master alloy ingot. Vertically rotating cylindrical mold preheated to 315°C was used to obtain samples of 60 mm in outer diameter, 6 mm in wall thickness and 110 mm in length. The mold was rotating under a centrifugal force magnitude of G=300, where G is the ratio of centrifugal force to that of the gravity [8]. According to the processing temperature, Al-Al_3Ti FGMs were made by CISM and CSPM techniques. In case of CSPM, the Al-5 mass%Ti master alloy, marked by dotted line in

Fig.1.1, was heated up to 800°C, which is lower than its liquidus temperature (1100 °C). On the other hand, CISM was carried out under the processing temperature of 1600°C which is above liquidus temperature of the master alloy as shown in Fig. 1.1. Then the melt was poured into the preheated cylindrical mold.

6.2.2. Microstructural observation

Samples for microstructural observation were cut from the FGM rings as shown in Fig. 6.1. Samples were mechanically polished and divided into five regions of equal intervals from the outer (1.0) to the inner (0.0) of the sample thickness (normalized distance). Microstructural characterization and intermetallics distribution were carried out using a scanning electron microscope (SEM) on plane OP2 of the fabricated FGMs, shown in Fig. 6.1.

6.2.3. Mechanical properties

Vickers hardness was measured at 0.49 N for 15 s. The hardness tests were carried out on plane OP2 from the outer to the inner surface of the sample. Wear property of the Al-Al_3Ti FGMs was evaluated using ball-on-disc type wear machine. Wear tests were carried out under reciprocal movement on planes OP1, OP2. The load and average sliding speed were 9.8N and 30 mm/s. Wear directions were perpendicular to the centrifugal force direction on both of OP1 and OP2.

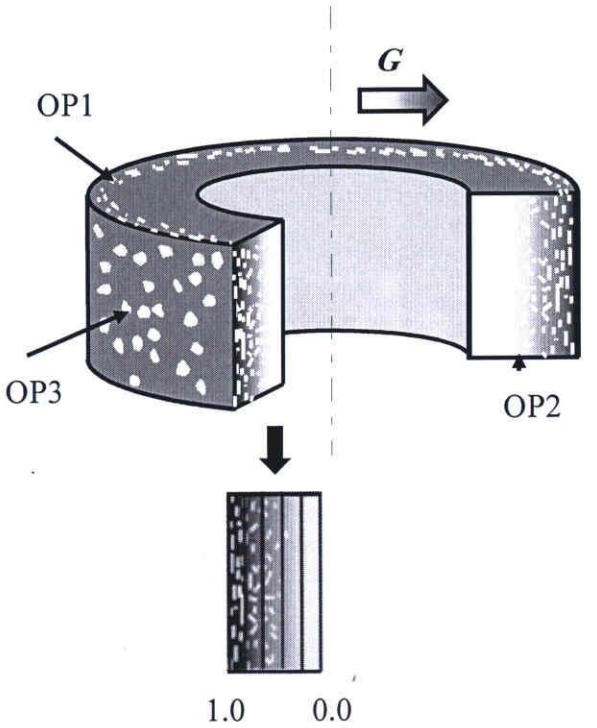

Fig. 6.1. Schematics for the FGMs ring and the sample cutting position.

6.3. Results and discussion

6.3.1. Microstructure of Al-Al_3Ti FGMs

Microstructures of Al-Al_3Ti FGMs fabricated by the CSPM and CISM are shown in Fig. 6.2. White phase in these micrographs is Al_3Ti particles. For both kinds of Al-Al_3Ti FGMs, Al_3Ti particles were gradually distributed from the outer to the inner surface of the sample. Fig. 6.3 shows variation of Al_3Ti particles volume fraction as a function of the normalized distance. The Al_3Ti particles distribution presents decreasing gradient from the outer to the inner surface. For Al-Al_3Ti FGMs fabricated by CISM, volume-fraction gradient of Al_3Ti particles in the intermetallics rich region is slower comparing with that of CSPM-FGMs. Since the applied centrifugal force was the same for the two methods, the slow compositional gradient obtained

in the CISM-FGMs is mainly due to the high processing temperature. In the current study, the average length of Al_3Ti particles in the CISM-FGMs ($\approx$ 57.2 μm) was larger than that of the CSPM-FGMs ($\approx$ 52 μm). This is due to the longer duration of cooling time caused by the high processing temperature of the CISM which encourages the growth of the Al_3Ti particles, taking into consideration that the mold preheating temperature and the centrifugal force magnitude were the same for the two methods.

In previous study, it has been reported that Al-Al_3Ti FGMs fabricated by CM has anisotropic wear property [7, 11]. According to this study, the anisotropic wear property comes from the alignment of Al_3Ti platelet particles due to the centrifugal force action. Because of it, the alignment of Al_3Ti platelet particle in Al-Al_3Ti FGMs is an important factor for the evaluation of its mechanical property. In order to investigate the alignment of Al_3Ti particle, orientation parameter, f_p, was calculated for Al-Al_3Ti FGMs fabricated by CISM and CSPM using equation (2-1) in section 2.3.1.

As defined in section 4.3.1.2, f_p [12-14] is equal to 1 for perfect alignment of the platelet perpendicular to the centrifugal force direction and becomes f_p=0 for random distribution of the platelets. The calculated f_p for both Al-Al_3Ti FGMs fabricated by CISM and CSPM were plotted in Fig.6.4. f_p values were calculated for the particles rich area in FGMs samples. From Fig. 6.4, f_p decreases toward the inner position. This is because Al_3Ti platelet particles are subjected to the moment caused by the angular velocity gradient of the melts along centrifugal force, and that this moment decreases toward the inner position [15]. Moreover, Al_3Ti particles in the outer surface of the CISM samples (1-0.8) have almost higher degree of alignment than those of CSPM. In previous study [16], it was observed that there is a position dependency of the orientation parameter along the centrifugal force direction in the fabricated FGMs. The orientation parameter increases towards the outer surface and the FGMs have an orientation parameter gradient. Higher orientation parameters were found with the increase in the volume fraction of Al_3Ti platelets. In addition to it, the longer duration of the semisolid state in case of the CISM is expected to give larger time for the orientation occurrence of Al_3Ti particles.

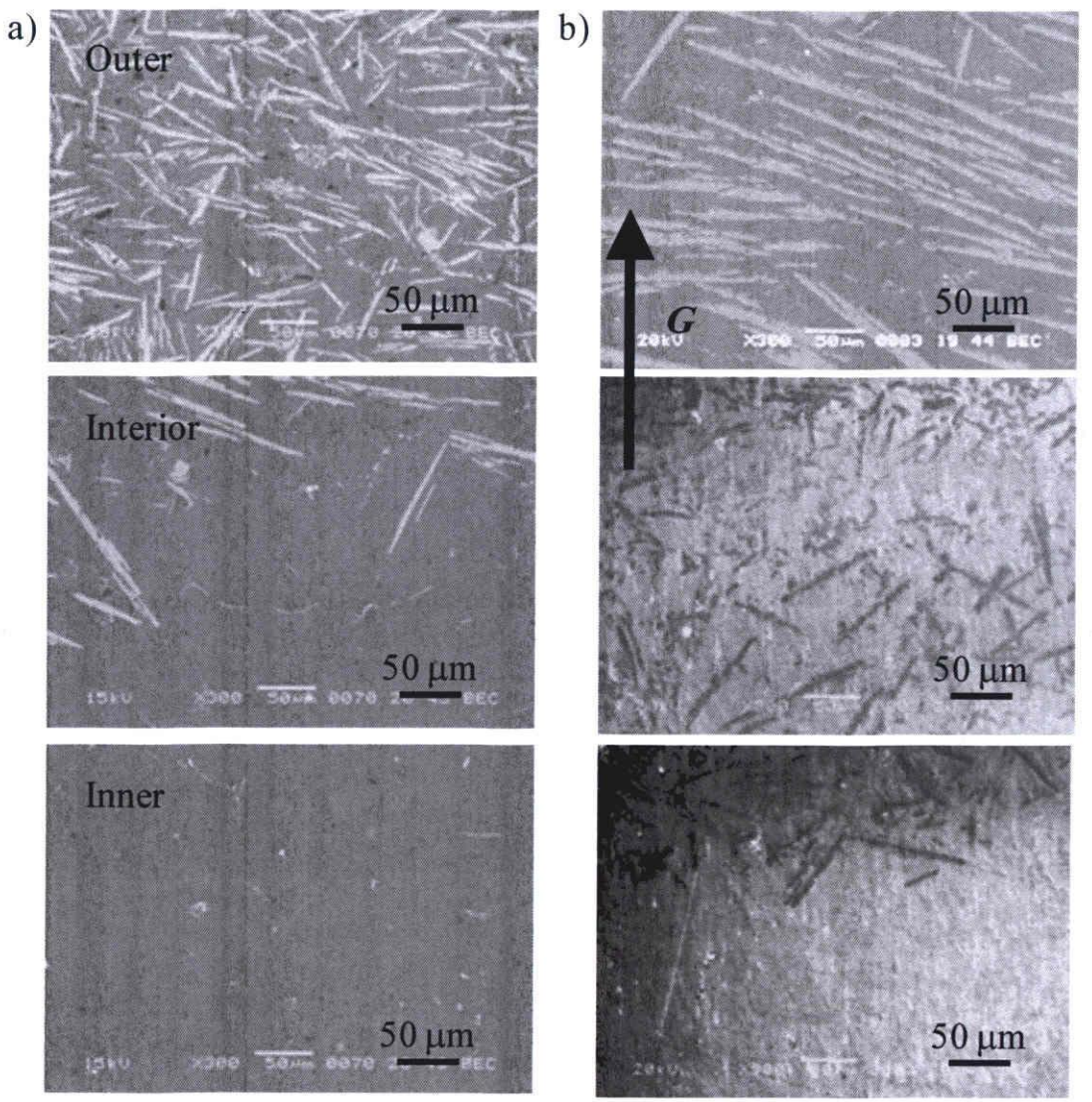

Fig. 6.2. SEM micrographs using compositional image showing microstructures of a) CSPM and b) CISM FGMs on plane OP2, near the outer, interior and inner surface.

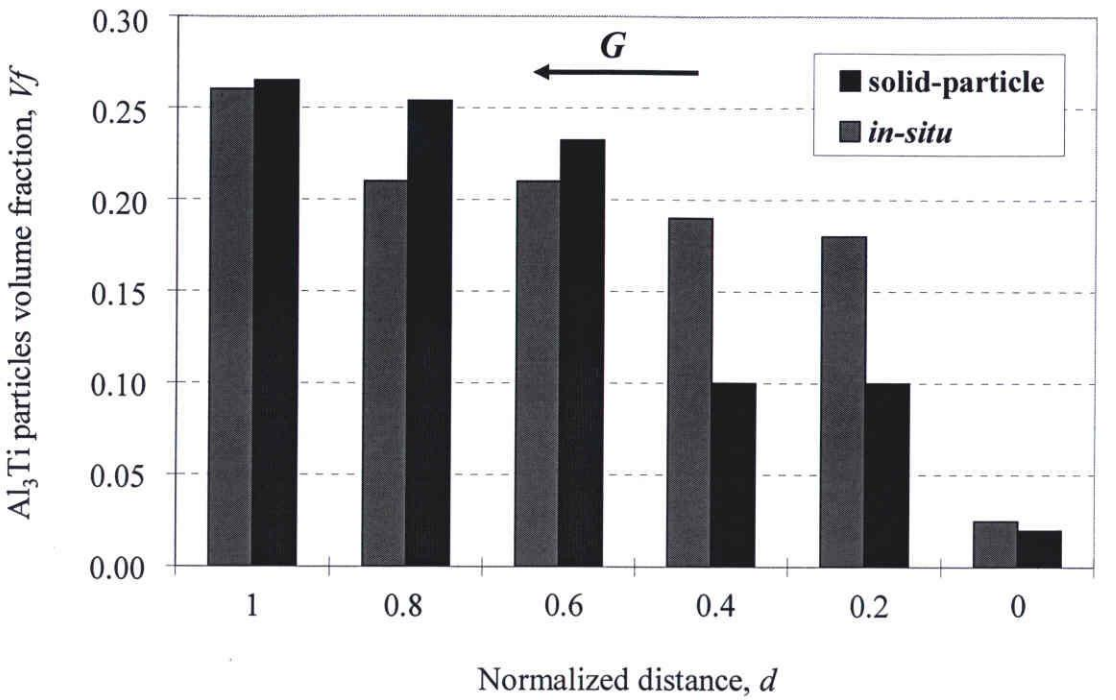

Fig. 6.3. Al_3Ti particles volume fraction distribution along sample thickness in CSPM and CISM FGMs.

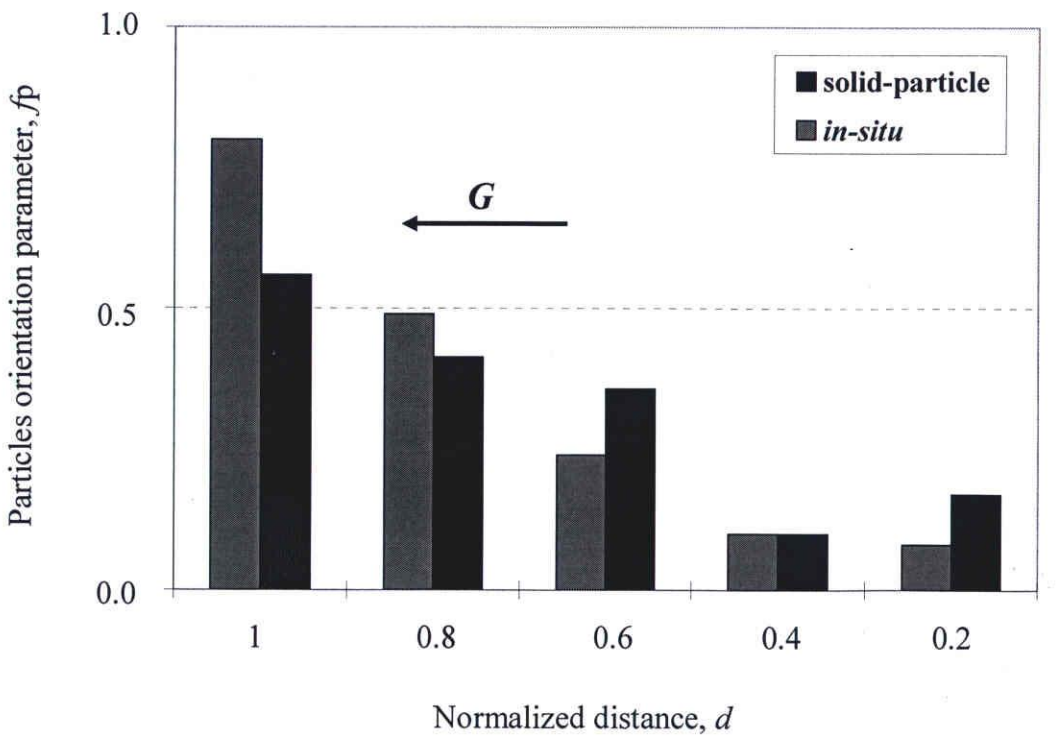

Fig.6.4. Orientation parameter distribution for CSPM and CISM samples on plane OP2.

6.3.2. Mechanical Properties

6.3.2.1. Hardness Distribution

Figure 6.5 represents the hardness distribution on plan OP2 in Fig. 6.1. The hardness distribution for the CSPM-FGMs shows a gradual decrease from the outer to the inner surface of the samples, which is in a good agreement with Al_3Ti volume fraction distribution. For the CISM-FGMs the hardness trend was slowly decreasing towards the inner surface of the ring and the relatively low Hv observed for the inner regions come from low particles volume fraction as shown in Fig. 6.3.

6.3.2.2. Wear property

Results of the wear test evaluated by weight loss are plotted in Fig. 6.6. As-cast Al-5 mass%Ti sample was also included as comparison. From this figure, it is found that CSPM-Al_3Ti FGMs samples have better wear resistance than that of the CISM specimens on both OP1 and OP2. As shown in Fig.6.3, volume fraction of Al_3Ti particles at normalized distance of 0.6, where wear tests were carried out, is larger in CSPM samples than in the CISM samples. Therefore, the wear property of CSPM samples is better than in the CISM samples.

In a study for Watanabe *et al.* [13], it was shown that the orientation profiles observed on OP1 are very similar to those along OP2. Namely, the orientation of Al_3Ti platelets has a three-dimensional correlation. According to the review of Watanabe *et al.* [11], the wear volume ratio increases together with the orientation parameter hence the anisotropy of wear resistance is emphasized with an increase in the orientation parameter of the Al_3Ti platelet. In the current experiments, since the wear direction for the aligned Al_3Ti particles is the same and the orientation profiles of OP1 are very similar to those along OP2, there is no difference between the wear on planes OP1 and OP2.

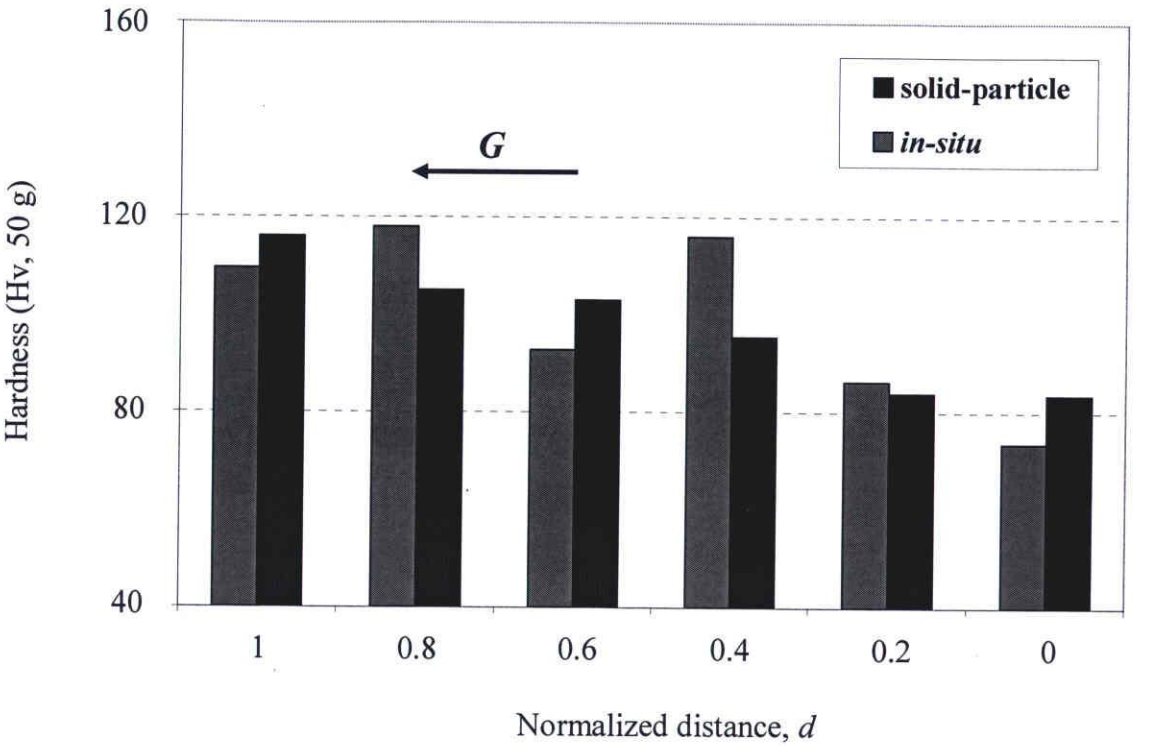

Fig.6.5. Hardness distributions for Al-Al_3Ti FGMs.

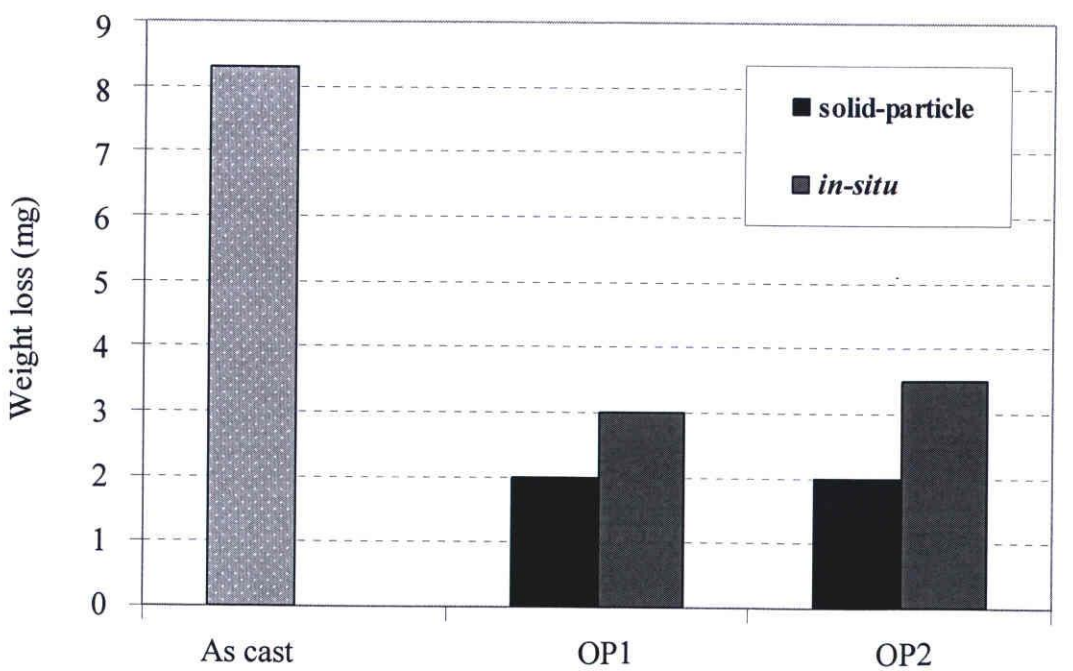

Fig. 6.6. Weight loss for Al-Al_3Ti FGMs samples, taken at two different planes, and the Al-5%Ti as cast sample.

6.4. Summary

Effects of fabricating Al-Al_3Ti FGMs by CM under different processing temperatures have been investigated. CISM-FGMs showed a slower compositional gradient and larger Al_3Ti particle size than that of CSPM-FGMs. The higher temperature in the CISM resulted in higher degree of Al_3Ti platelets orientation in the outer surface of the samples compared to those of CSPM. Al-Al_3Ti FGMs prepared by the two methods presented gradual hardness distribution from the outer to the inner surface of the sample. In general, solid-particle samples showed better wear resistance than the CISM-FGMs samples.

References:

[1] Fukui Y. JSME Int J Series III. 34, 1991, 144.

[2] Fukui Y, Takashima K, Ponton C.B. J. Mater. Sci., 29 (1994) 2281.

[3] Tijun C, Jian L, Yuan H. Res&Dev., 6 (2009) 319.

[4] Watanabe Y, Fukui Y. Formatex Microscopy Book Series., 2 (2004) 189.

[5] Watanabe Y, Sato H, Matsuda R, Fukui Y. Sci. Eng. Compos. Mater., 11 (2004) 185.

[6] Watanabe Y, Oike S. Acta Mater., 53 (2005) 1631.

[7] Watanabe Y, Sato H, Fukui Y. J. Solid Mech. Mater. Eng., 2 (2008) 842.

[8] Sequeira P.D. Ph.D Thesis, Nagoya Institute of Technology, (2006).

[9] Chawla N, Shen Y.L. Adv. Eng. Mater., 6 (2001) 357.

[10] Koczak M. J., Khatri S. C, Allison J. E., Bader M. G. Fundamentals of Metal Matrix Composites, edited by S. Suresh, A. Mortensen, A. Needleman), Butterworth-Heinemann, Stoneham, MA, 1993, p. 297.

[11] Watanabe Y, Sato H, Fukui Y. J. Solid Mech. Mater. Eng., 2 (2008) 842.

[12] Das S.K. Al-Rich Intermetallics in Aluminum Alloys. In: Westbrook J.H., Fleicher R.L. Editors. Intermetallic Compounds, Vol 3, Structural Applications of. NewYork, Wiley; 2000. p.175.

[13] Watanabe Y, Eryu H, Matsuura K, Acta Mater., 49 (2001) 775.

[14] McGee S.H, McCullough R.L. J. Appl. Phys., 55 (1984) 1394.

[15] Watanabe Y, Yamanaka N, Fukui Y, Z. Metallkd, 88 (1997) 717.

[16] Sequeira P.D, Watanabe Y, Eryu H, Yamamoto T, Matsuura K. Transactions of the ASME, J. Eng. Mater. Technol., **129**, No. 2, 304-312 (2007).

Chapter 7
Fabrication of Al-Ti System Functionally Graded Materials by Reaction Centrifugal Mixed-Powder Method

7.1. Introduction

Fabrication of Al-Al_3Ti functionally graded materials (FGMs) by the centrifugal method [1-5] was explained in section 1.2.2. The essential concept of CM is to make use of the difference in densities between the particles and the matrix, thus achieving the desired gradient by controlling the process variables [6-11]. Some of CM techniques are performed at temperatures lower than the liquidus temperature of the master alloy, named, centrifugal solid-particle method (CSPM) [1-8]. A detailed discription about the fabrication of Al-Al_3Zr FGMs using CSPM is present in chapter 4 of the current work. The other way is to process the FGMs by CM at a temperature exceeding that of the liquidus, known as, centrifugal *in-situ* method (CISM) [9-11]. More information about this high temperature CM is given in chapter 6, where Al-Al_3Ti FGMs was fabricated using both of CISM and CSPM.

Recently, centrifugal mixed-powder method (CMPM) was proposed by Watanabe *et al* [12] as a more practical choice for the fabrication of FGMs. In this method, a powder mixture of functional particles *B* and metal matrix particles *A* is inserted into a spinning mold. Then the metal matrix ingot *A* is melted and poured into the spinning mold containing the powder mixture. As a result, the molten metal matrix *A* penetrates into the space between the mixed powder (*A*+*B*) due to the centrifugal pressure. At the same time, the metal matrix particles *A* are melted by the heat from the molten matrix *A* poured from the crucible. Finally, an FGM ring with functional particles *B* distributed on its surface can be obtained. More detailed information about CMPM can be found elsewhere [12, 13].

In this study, a novel centrifugal method; reaction centrifugal mixed-powder method (RCMPM) was proposed to fabricate Al-Ti system FGMs under fixed centrifugal force. The main difference between our novel RCMPM and the recently proposed CMPM is that the formation of the reinforcement particles in RCMPM occurs during the mold spinning by

reaction. Namely, functional particles B and metal matrix A can be reacted as $xA + B = A_xB$. Therefore, the processing temperature at which the powder/molten metal matrix react to form the reinforcements is the essential point in our investigation. Since the RCMPM in the current experiments will be carried out under fixed centrifugal force, the produced compositional gradients will be mainly dependent on the processing temperature of the Al matrix melt. After preparation of the Al-Al_3Ti FGMs, the influence of the processing temperature on the formation of Al_3Ti intermetallic particles and their morphology and distribution in the fabricated FGMs have been investigated.

7.2. Experimental Procedures

7.2.1. Fabrication of Al-Al_3Ti FGMs by RCMPM

In the current study, Al-10 mass% Ti FGMs have been prepared using pure Ti powder and pure Al metal by a RCMPM. The schematics of the experimental procedures of RCMPM is shown in Fig. 7.1. In this study, a fine Ti powder is used for RCMPM instead of mixed powder. As a first step, the fine Ti powder (45 μm size) is inserted into the mold cavity prepared by the investment technique (Fig. 7.1(a)). The pure Al metal is then placed in the melting crucible surrounded by the induction coil. The processing temperatures varied between 1150°C and 1450°C. The liquidus temperature of the master alloy is about 1153°C as indicated on the Al-Ti partial phase diagram shown in Fig. 1.1 [14]. Once the Al melt reaches the desired temperature, the rotation starts while the Al melt filling the mold cavity penetrating into the spaces between the Ti particles as illustrated in Fig. 7.1(b). Thus causing a partial/complete melting of the Ti particles allowing the occurence of Al/Ti reaction layer on the Ti particles surface, as shown in Fig. 7.1(c). Finally, Al_xTi intermetallic compounds are formed and distributed through the sample length depending on the Al melt temperature (Fig. 7.1(d)). The applied centrifugal force magnitude of G= 80 was used in the current experiments, where G number is the ratio of centrifugal force to that of gravity. The centrifugal force direction and flowing direction of the molten metal are presented in Fig. 7.2. Figure 7.3 shows fabricated Al-Al_3Ti FGM sample. The

prepared Al-Al_3Ti FGM samples were cut in a direction normal to *G* force from the positions shown in Fig. 7.3.

7.2.2. Investigation of Al-Al_3Ti FGMs

The Al-Al_3Ti FGMs microstructure has been observed using scanning electron microscope (SEM). Two distances were identified in the observed samples: the first one starts at 10 mm from the sample tip and up to 35 mm towards the end (where the Al_3Ti particles present in a defined form-named W in Fig. 7.3). The second distance starts from the sample tip and ends at 35 mm (named Z in Fig. 7.3). The former distance was used to quantify Al_3Ti particles length and their volume fraction distribution while the later distance used for hardness measurements. The average Al_3Ti particles length was then measured at every 5 mm of the specified distance using the linear intercept method on randomly taken SEM micrographs. The Al_3Ti particles volume fraction was quantitatively calculated by considering the area fraction of the Al_3Ti particles. The formation of Al_3Ti was investigated using energy dispersive spectroscopy (EDS) point analysis and X-ray diffraction (XRD) patterns. The hardness distribution in the fabricated Al-Al_3Ti FGM samples was evaluated along the distance, Z, by a 5mm step. Vickers microhardness tester at 3 N for 15 s was used for the measurements.

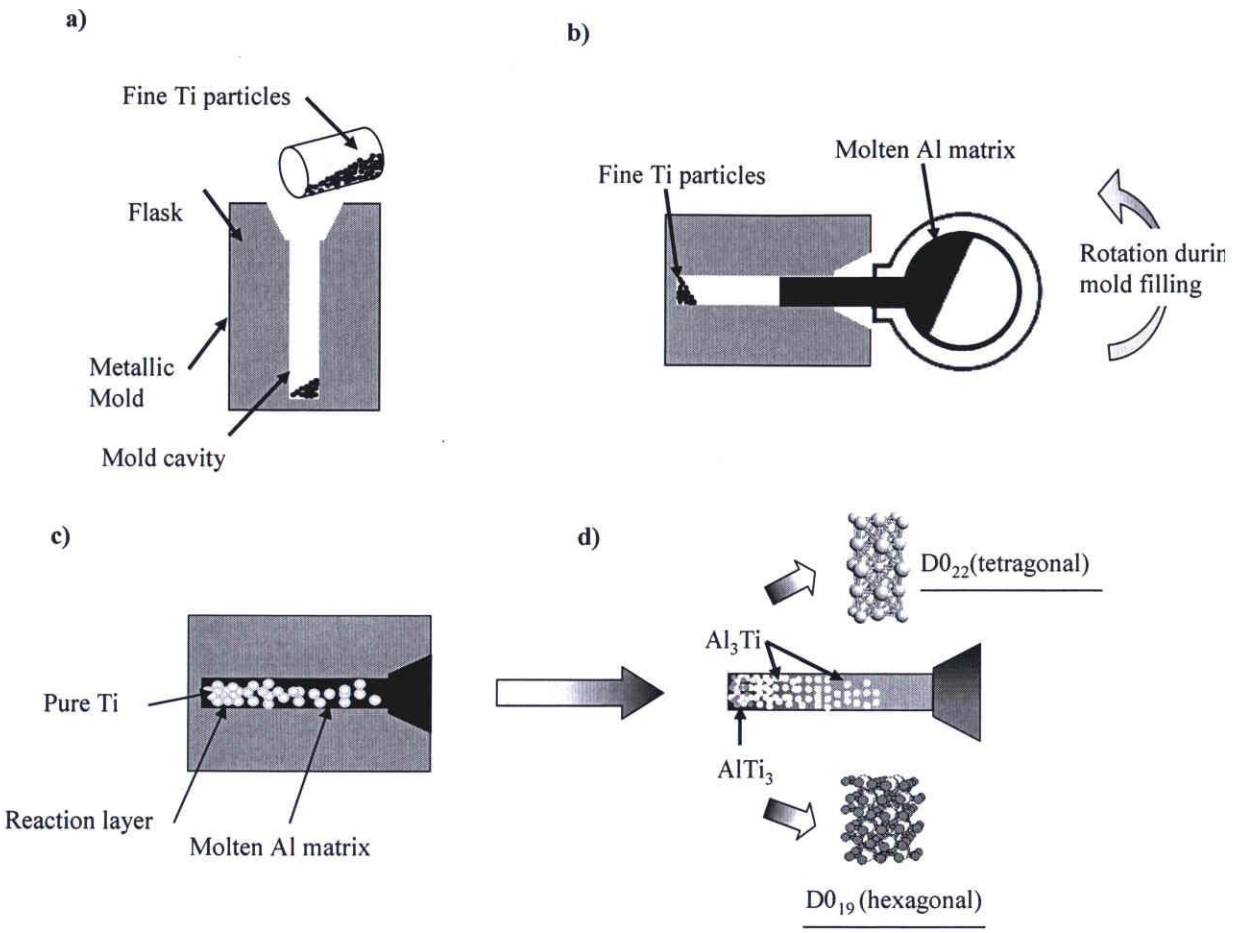

Fig. 7.1. A schematic illustration showing the process of the reaction centrifugal mixed-powder method (RCMPM).

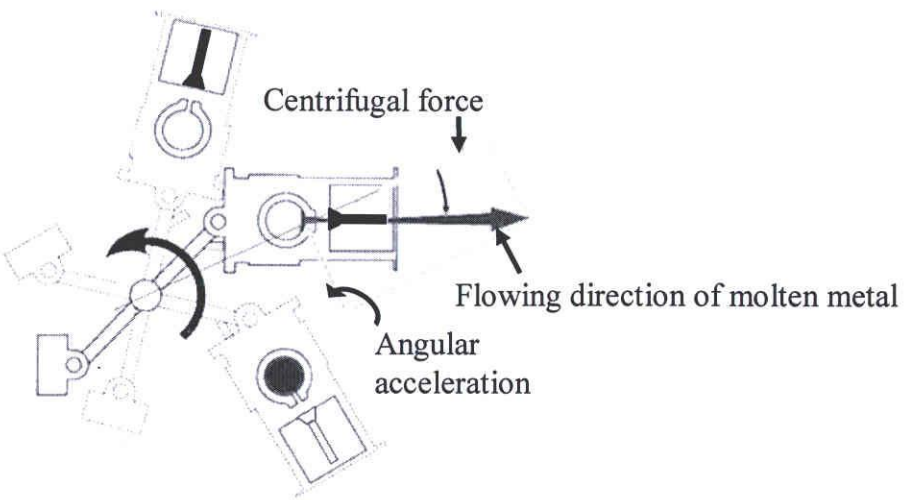

Fig. 7.2. The centrifugal force direction and flowing direction of the molten metal.

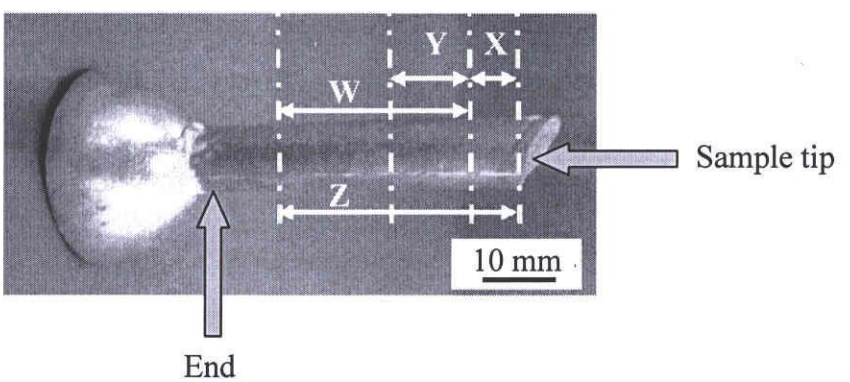

Fig. 7.3. As fabricated Al-Al_3Ti FGM sample.

7.3. Results and Discussion

7.3.1 Microstructure of Al-Al_3Ti FGMs

The formation of intermetallics in Al-Ti system is mainly a temperature dependent process. As a result, the microstructure of the fabricated Al-Al_3Ti FGMs showed a significant change with the processing temperature of the Al melt. In the current study Al-Al_3Ti FGMs were fabricated at three temperature levels: lower than the liquidus temperature of the master alloy (1150°C), relatively higher temperature (1250°C) and the high temperature versions (1350°C and 1450°C). Since the experiments were carried out under a fixed centrifugal force (G = 80), main processing parameter affecting the particles size and morphology will be the casting temperature.

Figure 7.4 shows the SEM micrograph and the corresponding Al and Ti maps of Al-Al_3Ti FGM prepared at 1150°C. At RCMPM processing temperature of 1150°C, the reaction between Al/Ti proceeded and Al_3Ti intermetallic could be formed at part Y of the samples as shown in Fig. 7.4. The very fine particles observed in this figure are identified to be Al_3Ti particles which are ununiformally dispersed in the Al matrix, while the white particles in the magnified microstructure are unreacted Ti as has been verified using the EDS. The size of these granular Al_3Ti particles was in order of (6-12 μm). However, the observed granular shape of the Al_3Ti particles was different than its reported platelet morphology [1-5]. This is because of the Al melt temperature which was actually 1150°C when being in the crucible surrounded by the induction coil. This temperature was relatively reduced when the Al melt contacted the Ti particles at the end of the mold cavity. This is why the unreacted Ti particle has been observed.The presence of some unreacted Ti particle in the matrix indicating that not all the added Ti could react and form Al_3Ti at the specified temperature. The corresponding XRD pattern of part Y of Al-Al_3Ti FGM prepared at 1150°C is shown in Fig. 7.5. Some Ti peaks could be remarked along with Al_3Ti peaks. The thickness of part Y containing such structure was roughly 12 mm and the rest of the sample was pure Al.

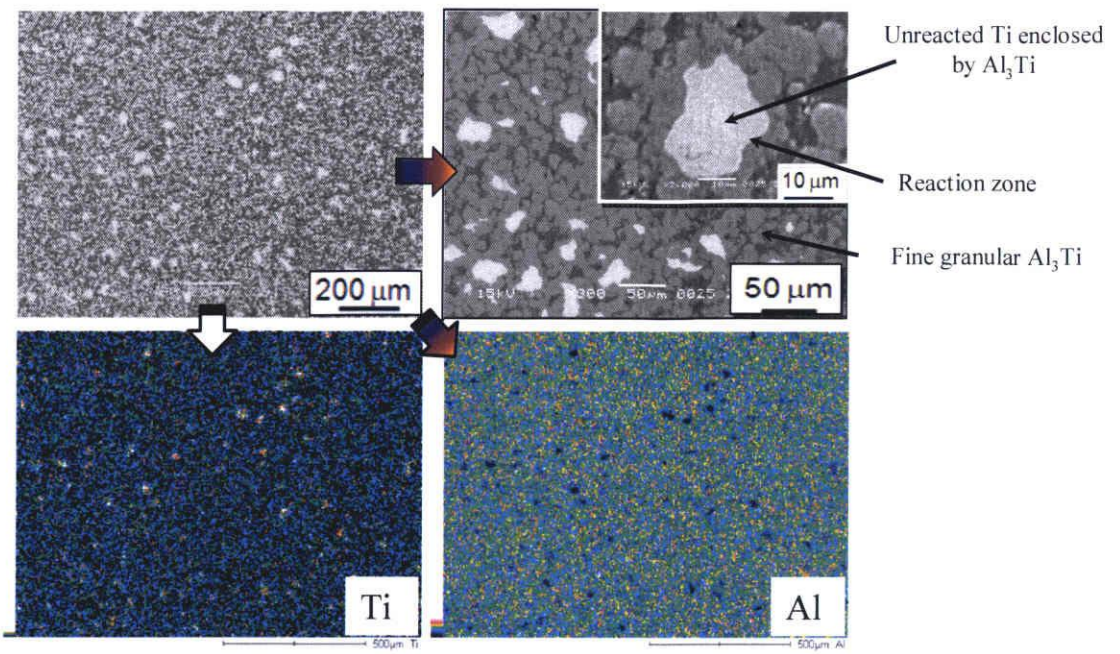

Fig. 7.4. The SEM micrograph of Al-Al_3Ti FGMs prepared at 1150 °C and the corresponding Al and Ti maps.

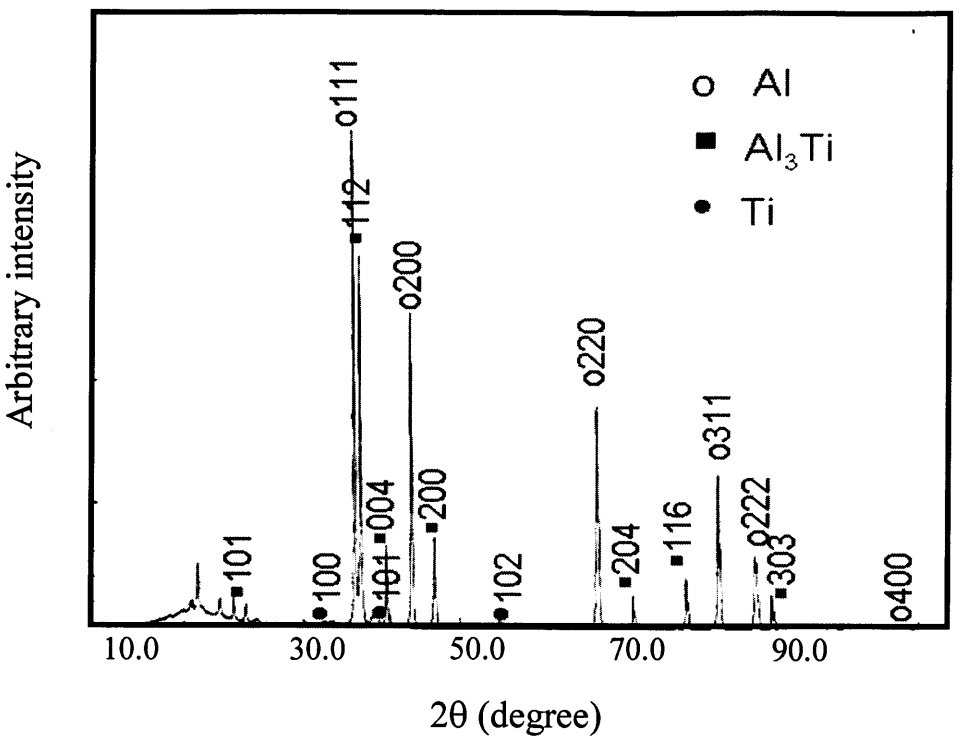

Fig. 7.5. The XRD pattern of part Y of Al-Al_3Ti FGM prepared at 1150 °C.

The SEM micrographs of part Y of the FGMs prepared at different processing temperatures are shown in Fig. 7.6. The FGM sample fabricated at 1150°C containing fine granular particles is shown in Fig. 7.6 (a). Upon increasing the melting temperature to 1250°C, these fine granular Al_3Ti particles were first formed at part Y with 10 mm thickness then the coarse platelet-shaped Al_3Ti particles could be obtained next to it, as shown in Fig. 7.6 (b). The formation of the platelet-shaped particles next to the granular one can be explained as follows; when the Al melt contacts the Ti powder some Al_3Ti granular particles could be formed. Since the heat of formation for Al_3Ti at 25°C is -35.6 kJ/g atom [15], the adiabatic temperature rise due to the formation of Al_3Ti was approximated to be ~1127 °C by taking the heat capacity as ~25 J/(K mol) [15]. This heat release due to the exothermic reaction can raise the temperature and accelerate the Al/Ti reaction enabling the formation of coarse Al_3Ti platelets in the following regions [16].

Though the exothermic reaction to form Al_3Ti occurs close to the tip as well, the following regions still have higher temperature due to the increased heat loss from molten Al to the surrounding when reaches the sample tip. Moreover, the faster cooling rate in the tip region can also support the formation of such fine granular particles. Since the equilibrium shape of Al_3Ti phase is platelets, the platelet shaped Al_3Ti phase can be observed for the FGM fabricated at higher processing temperatures. In addition, the high temperature processing enables the Al/Ti complete reaction thus allowing the Al_3Ti particles to form in its equilibrium shape. Based on it, once the coarse particles formed, it will be placed next to the fine particles under the action of the applied centrifugal force.

Figure 7.7 and Table 7.1 present the results of point analysis of FGM sample fabricated at 1250°C. The average composition of both the fine and coarse Al_3Ti particles was estimated to be similar to that of Al_3Ti. This confirms that the difference between the coarse platelet particles and the fine granular particles is only in their morphology not in their chemical composition.

The typical Al-Al_3Ti FGM containing platelet Al_3Ti particles could be obtained at 1350°C as clear from Fig. 7.6 (c). Further increase of the RCMPM temperature did not show a significant change in the microstructure, except for the coarser Al_3Ti platelet particles observed for the FGM sample fabricated at 1450°C, as presented in Fig. 7.6 (d).

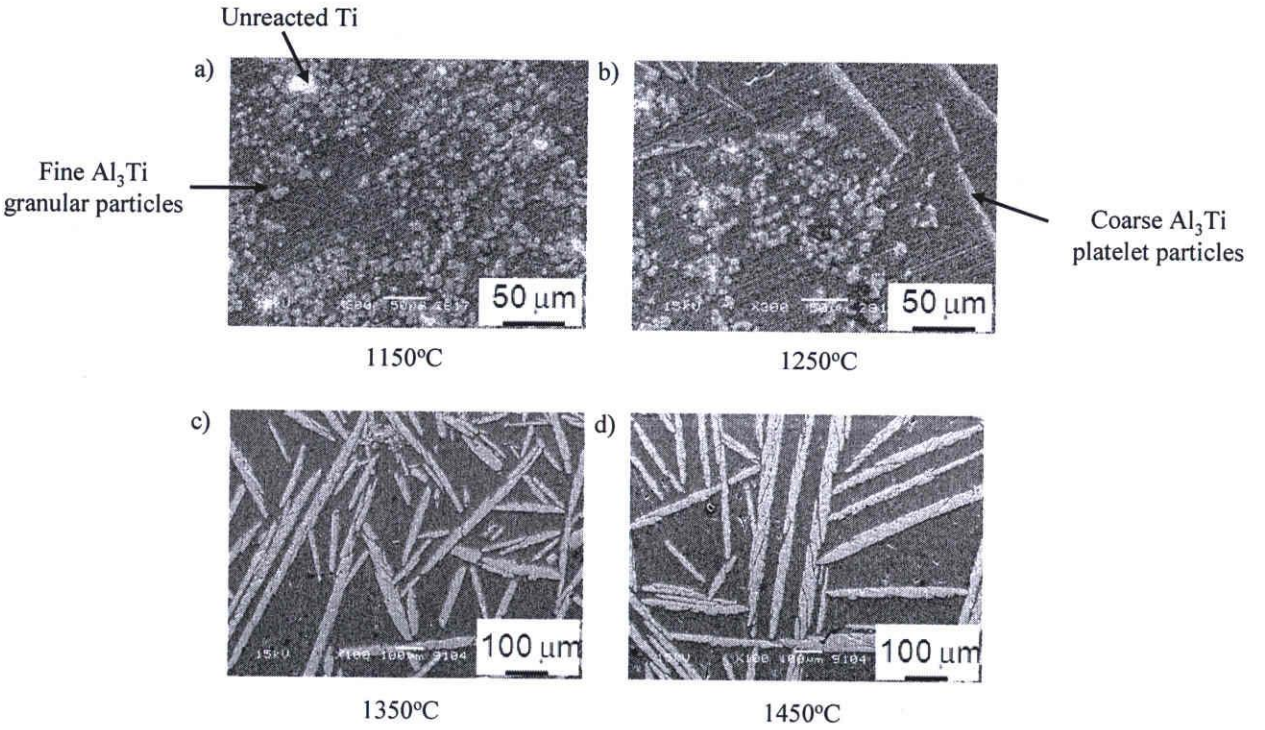

Fig. 7.6. The SEM micrographs of part Y of the FGMs prepared at different processing temperatures.

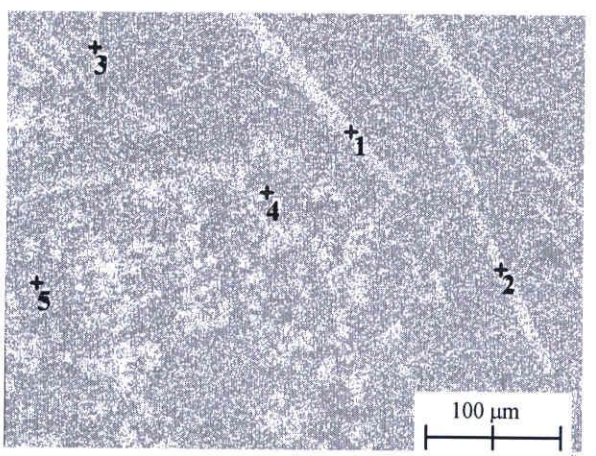

Fig. 7.7. The SEM micrograph used for point analysis belongs to (1250°C) FGM samples.

Table 7.1. Point analysis data correspond to Fig. 7.7.

Position	Atomic % Al	Atomic % Ti
Point 1	73.28	26.72
Point 2	73.97	26.03
Point 3	78.82	21.18
Point 4	83.46	16.54
Point 5	76.51	23.49

7.3.2 Particles length and volume fraction distributions in Al-Al_3Ti FGMs

The centrifugal casting processing temperature in some reported studies showed a remarkable effect on the intermetallic particles distribution in the fabricated FGMs [17]. In the current experiment, the processing temperature of the Al-Al_3Ti FGMs showed a strong influence not only on the Al_3Ti particles shape but also on the distribution of Al_3Ti particles size and volume fraction. Figure 7.8 shows the Al_3Ti particles volume fraction distribution in the fabricated samples. As described in section 7.3.1, the Al_3Ti fine granular particles were present up to 12 mm next to part X (20 mm from the tip) in case of 1150°C sample and the rest was pure Al. This particle distribution can be described as steep gradient considering the sample length (the sample length was 50 mm). The thickness of this layer containing the granular particles was then decreased to about 10 mm (15 mm from the tip) when the Al melt temperature increased to 1250°C and some platelet shaped Al_3Ti particles could be obtained up to the sample end. This can be clearly understood from the slower volume fraction distribution of sample fabricated at 1250°C compared to that of 1150°C. With further increase of the processing temperature, the distribution gradient of Al_3Ti platelet particles in this high temperature samples becomes more gentle from the sample tip up to end. In addition, the increase in the particles length when changed from granular to platelet morphology was further

confirmed by the Al_3Ti particles length distribution shown in Fig. 7.9. Upon further heating of the Al melt up to 1350°C, the occurrence of the coarse particles was more frequent and the granular morphology was rarely observed. Increasing the temperature up to 1450°C resulted in absence of these low temperature fine particles and only coarse Al_3Ti platelet particles could be found up to the end of the FGM sample as shown in Fig. 7.9. The slower particles distribution gradient observed at higher temperature is in accordance with the reported work of the FGMs fabricated by CISM [17].

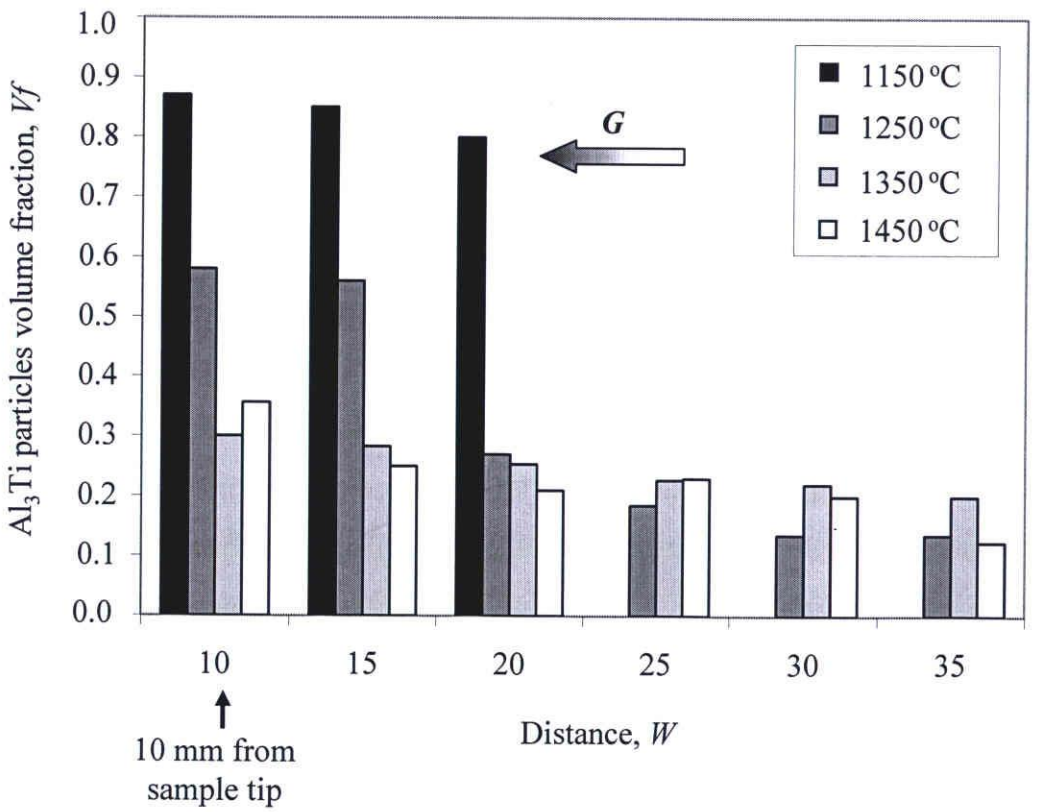

Fig. 7.8. Al_3Ti particle volume fraction distribution at different processing temperatures.

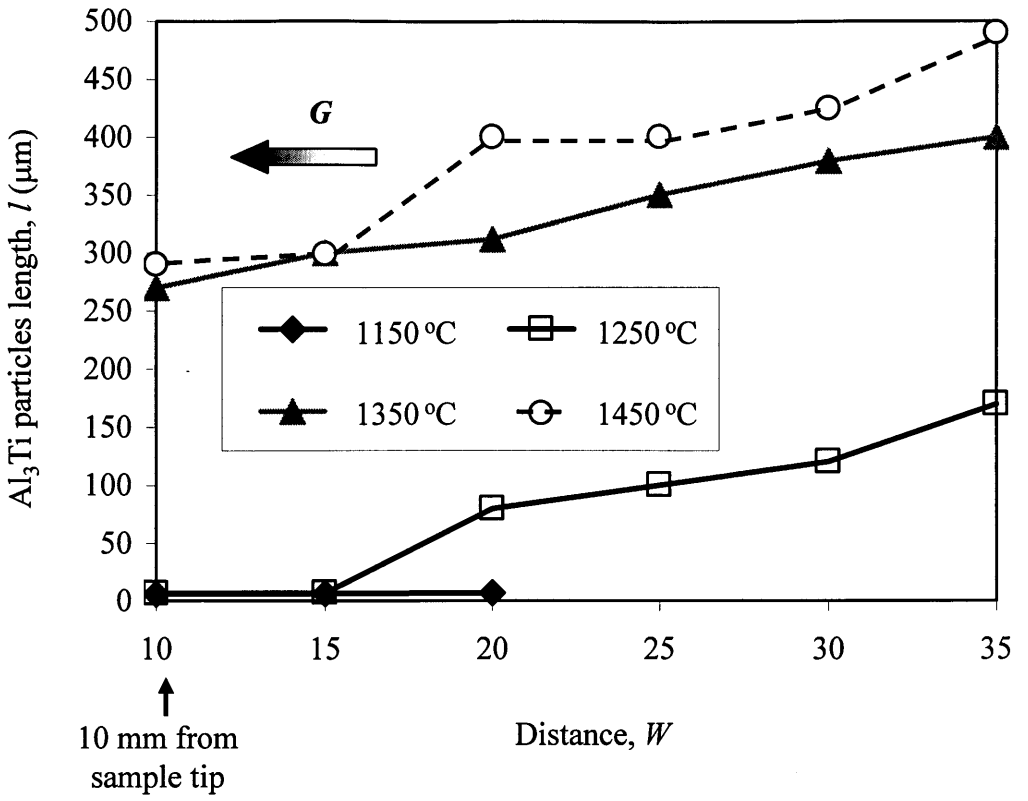

Fig. 7.9. Distribution of Al_3Ti particles length at different casting temperatures.

The formation of graded composition in the current FGM samples can occurs through two mechanisms. At 1150°C, which is just below the liquidus of the master alloy (1153°C), the centrifugal process is considered CSPM, in this case the formation of graded composition is believed to occur due to the density difference between Al_3Ti and liquid Al. However, upon increasing the processing temperature, another mechanism is suggested [11]. This is the formation mechanism of the graded composition in case of A–B alloy *in situ* FGM under the centrifugal force, which can be summarized according to Watanabe and Oike [11] as follows:

1. Due to the density difference, partial separation of Al (2.261 Mg/m^3 at 1100°C) and Ti (4.1 Mg/m^3at 1680°C) elements in the liquid state occur.
2. A chemical composition gradient is formed before the crystallization of primary crystals.
3. The primary crystal in the matrix appears to depend on local chemical composition.

4. The primary crystal migrates according to density difference, and a further compositional gradient is formed.

Concluding, the Al_3Ti compound formation depends on the processing temperature, so its migration and distribution would be temperature dependent processes as well.

7.3.3 Formation mechanism of Al_3Ti/Ti_3Al at the processing temperature

In the Al-Ti phase diagram, formation of various long-period structures has been reported in the Al-rich region deviating from the stoichiometry. Also the peritectic reaction accompanying the formation of Al_3Ti and the high-temperature and low-temperature modifications of Al_3Ti exist [18, 19, 20]. In a recent study, the synthesis of the elemental nanoscaled Al/Ti multilayer has been investigated [21]. The thickness of layers was obtained by plasma-assisted magnetron layer-by-layer sputtering. Due to the diffusion of Ti through the Al/amorphous interface, the slowly heated synthesis between Ti and Al completed below 700°C. The complex solid-state reaction between Al and Ti in that study was explained as a sequence of gradual changes; it starts by amorphisation, then the metastable c-Al_3Ti is formed, and is progressively changed to tetragonal Al_3Ti, Al_2Ti and finally AlTi and also Ti_3Al phases [21].

Concluding, it is difficult to reach the equilibrium state at low temperatures within a limited time, certain confusion might accompany the process of formation and thermal stability of the individual phases due to the processing techniques as analyzed in the review of Schuster and Palm [22]. Considering the aforementioned works, in our current study, where different processing temperatures were used and relatively rapid cooling was present (sample thickness = 8 mm), it is expected that some other compounds rather than Al_3Ti can be formed.

Figure 7.10 is SEM micrographs and the corresponding Ti and Al maps showing the microstructure close to the tip of the sample processed at 1350°C. The structure of this part, named part X in Fig. 7.3, include a Ti matrix containing very fine Ti_3Al particles and irregulary shaped Al_3Ti particles. The EDS points analysis performed on this sample is shown in Fig. 7.11 and Table 7.2. For further analysis, the XRD pattern of the sample processed at 1350°C was investigated and presented in Fig. 7.12. From this figure, the high Al_3Ti peaks can be observed along with small Ti_3Al peaks thus confirming the formation of Ti_3Al intermetallic compound as

well as Al_3Ti at the processing temperature using our current method. The thickness of the layer containing Ti_3Al decreased from about X= 8 mm in case of 1150°C samples to X= 3 mm when the Al melt temperature increased to 1450°C. This is due to the occurence of complete reaction between the Ti and Al at higher processing temperatures. Next to part X of the sample, some Al_3Ti could be sucessfuly formed as shown in Fig. 7.13 of sample fabricated at 1350°C as an example. The shape of these Al_3Ti particles and their distribution were dependent on both the position and the casting temperature as discussed in the previous section.

It was observed that Ti_3Al intermetallic compound could be formed close to the FGM sample tip, where the Al melt temperature is lower than the rest of the sample due to the heat loss to the surrounding. It was reported that both of Al_3Ti and Ti_3Al can be described as one-dimensional antiphase domain structure (1D-APS) [23]. Al_3Ti has the $D0_{22}$ structure, which is tetragonal with space group of I $4/m^3$ and the lattice parameters of the $D0_{22}$ are; a= 3.84 Å and c= 8.59 Å [24]. On the other hand, Ti_3Al has a $D0_{19}$ hexagonal structure of a= 5.614 Å and c= 4.665 Å [25]. Following the reported experimental research and theoretical calculations [20], it is supposed that the formation of the Ti_3Al-like (1D -APS) structure are both kinetically and thermodynamically simple and preferred relatively to the other Al-Ti rich phases. If the Al-rich Al-Ti alloys are in non-equilibrium conditions (rapid quenching, severe mechanical treatment,...), the 1D -APSs might be formed first before the stable thermodynamic phases [20].

In the current experiment, there is a particular increase of the thermodynamic potential by centrifugal force. This is because the pressure exerted by centrifugal force is proportionally related to the internal energy of the thermodynamic system as reported earlier [26, 27]. Since the maximum pressure exerted by the centrifugal force will be on the flask bottom (named sample tip in Fig. 7.3) while the minimum pressure will be in the button then the thermodynamic conditions will be different between the two parts. Furthermore, the melt temperature at the sample tip will be relatively lower compared to the next parts of the sample. Accordingly, some compounds rather than Al_3Ti can be formed close to the sample tip. Once formed, all the Al/Ti reaction produced particles will be inhomogeneously distributed along the sample length depending on the exerted centrifugal pressure. Therefore, compounds like Ti_3Al

could be formed near the tip in the Al-Ti system FGM samples and coexisted with irregularly shaped Al_3Ti particles.

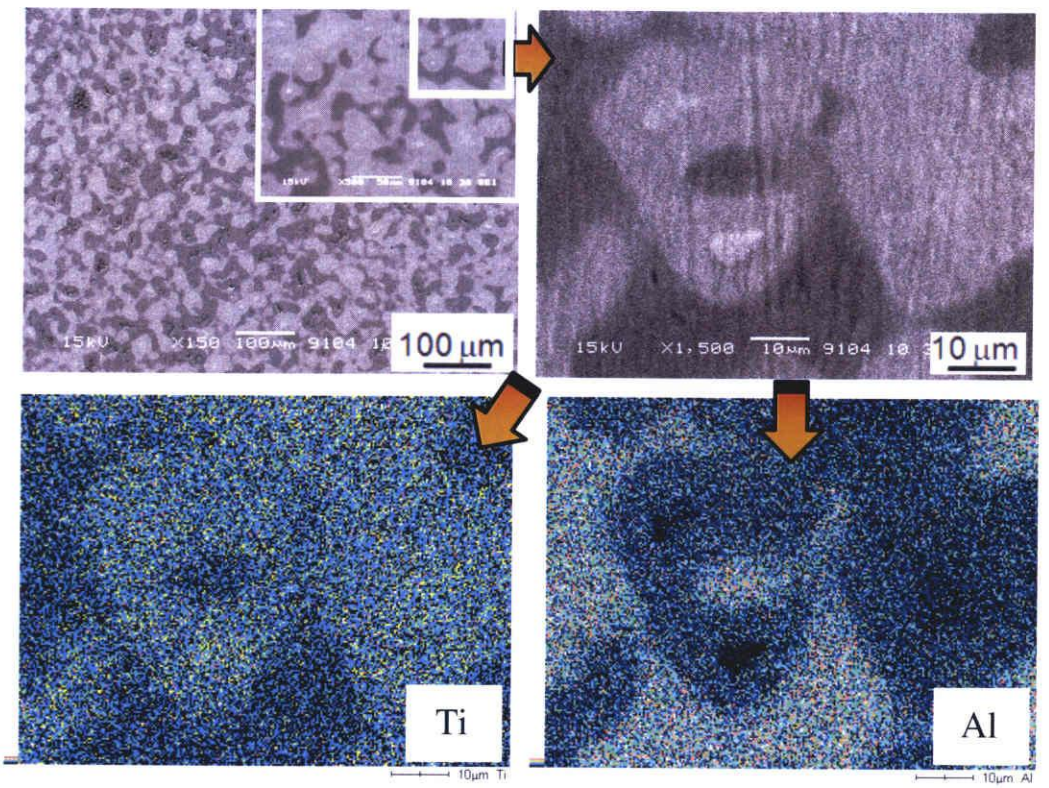

Fig. 7.10. SEM micrograph showing the microstructure close to the tip of the specimen processed at 1350°C and the corresponding Ti and Al maps.

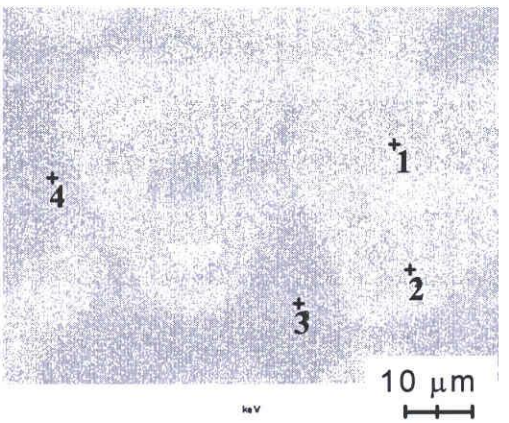

Fig.7.11. SEM micrograph used for EDS point analys on part X of the 1350°C sample.

Table 7.2. Point analysis data correspond to Fig. 7.11.

Position	**Atomic % Al**	**Atomic % Ti**
Point 1	29.11	70.89
Point 2	33.28	66.72
Point 3	72.35	27.65
Point 4	71.63	28.37

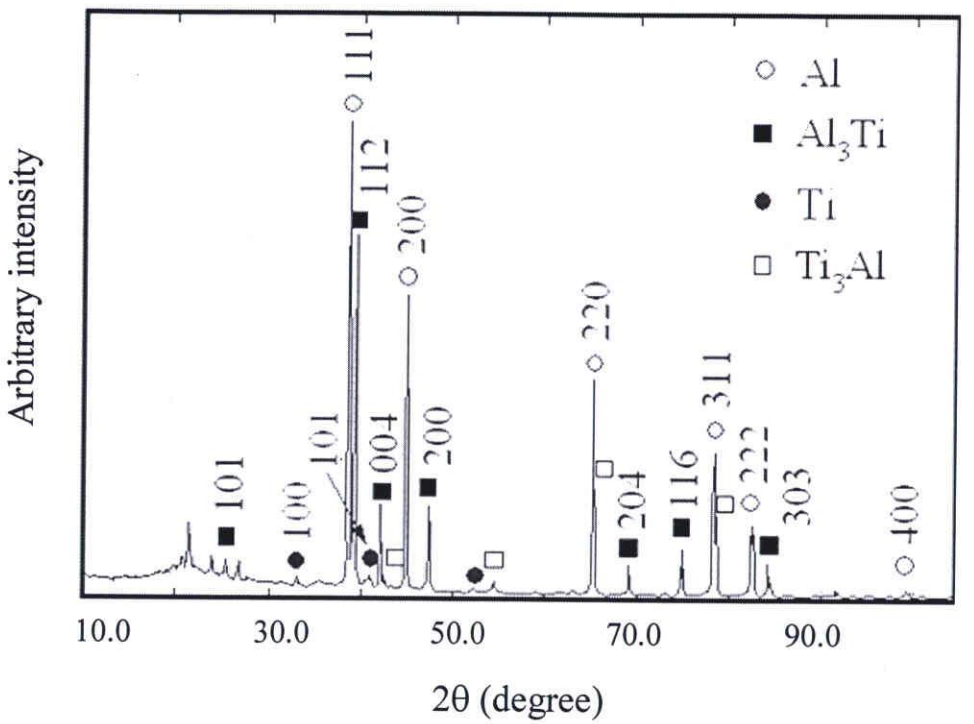

Fig. 7.12. The X-ray diffraction pattern of the sample processed at 1350 °C.

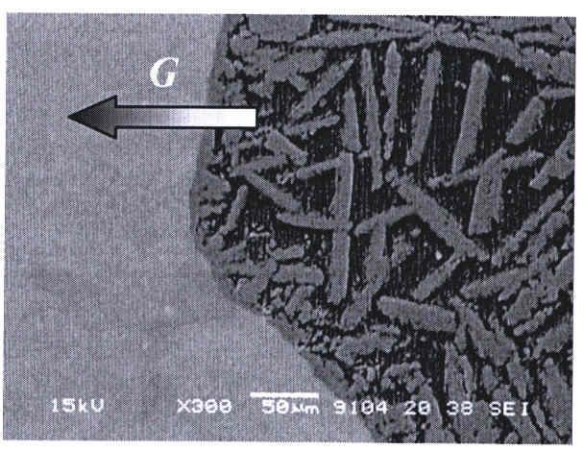

Fig. 7.13. Microstructure next to part X of the 1350°C sample where some Al_3Ti platelets could be successfully formed.

7.3.4 Hardness distribution

Figure 7.14 shows the hardness distribution from the sample tip and up to 35 mm of its length. In this figure, it is obvious that the sample tip has very high hardness compared to the rest of the sample. It is believed that the presence of very fine Ti_3Al particles in the matrix has enhanced the hardness close to the tip.This in its turn resulted in a steep distribution of the hardness at all the processing temperatures. Following this part, the fine granular Al_3Ti particles shown in Fig. 7.6 were present at 1150°C and 1250°C casting temperatures. Therefore the hardness of the samples containing such fine particles ranged between 78 Hv and 110 Hv, which is significantly higher than the hardness of the Al-Al_3Ti FGMs observed in chapter 6. This is due to the presence of Al_3Ti intermetallics as fine granular particles compared to our reported coarse Al_3Ti platelets. Once the Al_3Ti particles formed with its platelet shape, the hardness of 1250°C samples decreased again up to the sample end. When the casting temperature increased to 1350°C and 1450°C, the coarse Al_3Ti particles formed and lower hardness values have been observed. The gradient distribution of the hardness in the fabricated FGMs was in accordance with the particles volume fraction distribution shown in Fig. 7.8 and the particles size gradient shown in Fig. 7.9.

The hardness distribution in the FGMs fabricated by CM depends mainly on the particles distribution gradient. A slower hardness distribution has been recorded for Al-Al_3Ti FGM rings fabricated by the CISM, as previously shown in section 6.3.2. This is because of the more gradual occurrence of Al_3Ti particles from the sample outer surface and up to its interior in case of CISM [11, 17]. In the experiments of chapter 6, the Al-Al_3Ti FGMs have been fabricated from an Al-5 mass% Ti ingot, therefore the hardness distribution was related only to the particles volume fraction. However, in the current RCMPM experiments the FGMs have been made using Ti powder and Al melt, thus formation of Al_3Ti intermetallics occured during the casting process. Considering it, there are three parameters can influence the hardness distribution in the present Al-Ti system FGMs: formation of the intermetallic particles, the particles characteristics (shape and size) and the particles distribution gradient at the processing temperature.

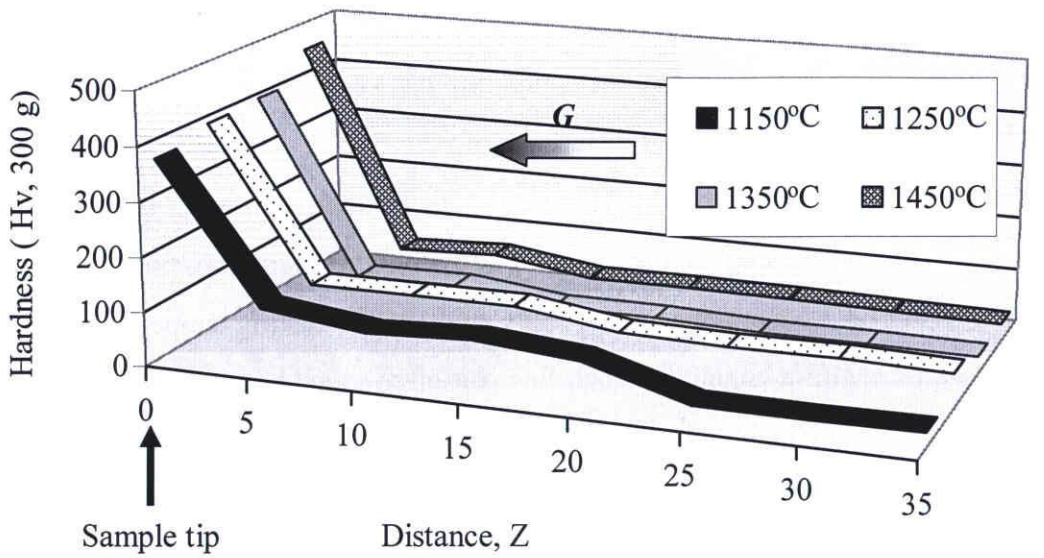

Fig. 7.14. Vickers hardness distribution at different processing temperatures..

7.4. Conclusions

In the current study, the Al-Ti system FGMs produced by RCMPM showed a slower particles distribution at higher casting temperatures. In addition, formation of Al_3Ti intermetallics and its morphology showed a significant change when processed at different temperatures relative to the liquidus temperature of the master alloy. At relatively lower temperatures (1150°C-1250°C), fine granular Al_3Ti particles could be observed. Moreover, Ti_3Al intermetallic compound and un-reacted Ti phases are found for the sample fabricated at lower processing temperature. These granular Al_3Ti particles could not be found at higher processing temperatures (1350°C), where only coarse Al_3Ti platelet particles were obtained. Casting at higher temperature (1450°C) resulted in more coarsening of the Al_3Ti platelets. The hardness distribution in the fabricated FGMs showed a clear dependency on both the particles type, their size and their distribution at the processing temperature.

References:

[1] Watanabe Y, Yamanaka N, Fukui Y. Z. Metallkd., 88 (1997) 717.

[2] Watanabe Y, Yamanaka N, Fukui Y. Metall. Mater. Trans., 30A (1999) 3253.

[3] Watanabe Y, Eryu H, Matsuura K. Acta Mater., 49 (2001) 775.

[4] Sequeira P.D, Watanabe Y, Y. Fukui. Scripta Mater., 53 (2005) 687.

[5] Sequeira P.D, Watanabe Y, Eryu H, Yamamoto T, Matsuura K. J. Eng. Mater. Tech. Trans. ASME, 129 (2007) 304.

[6] Fukui Y. JSME Inst. J. Series III 34 (1991) 144.

[7] Watanabe Y, Yamanaka N, Fukui Y. Composites Part A, 29 **A** (1998) 595.

[8] Watanabe Y, Kawamoto K, Matsuda K. Comp. Sci. Tech., 62 (2002) 881.

[9] Yamagiwa K, Watanabe Y, Fukui Y, Kapranos P. Mater. Trans., 44 (2003) 2461.

[10] Watanabe Y, Sato R, Matsuda K, Fukui Y. Sci. Eng. Comp. Mater., 11 (2004) 185.

[11] Watanabe Y, Oike S. Acta Mater. 53 (2005) 1631.

[12] Watanabe Y, Inaguma Y, Sato H, Miura-Fujiwara E. Materials, 2 (2009) 2510.

[13] Watanabe Y, Miura-Fujiwara E, Sato H. J. Jpn. Soc. Powder Powder Metall., 57 (2010) 321 [in Japanese].

[14] Massalki T. B, Murray J. L, Bennet L. H, Baker H. Binary Alloy Phase Diagrams, ASM (1986).

[15] Gale W.F, Totemeier T.C. Smithells metals reference book. 8th ed. Elsevier; 2004.

[16] Hsu C.J, Chang C.Y, Kao P.W, Ho N.J, Chang C.P. Acta Mater., 54 (2006) 5241.

[17] Watanabe Y, Fukui Y. FORMATEX Microscopy Book Series. 2 (2004)189.

[18] Illekova E, Svec P, Janickovic D. The 13th International Conference on Rapidly Quenched and metastable materials, Journal of Physics: Conference Series, 144 (2009)1.

[19] Stein F, Zhang L, Sauthoff G, Palm M. Acta Mater., 49 (2001) 2919.

[20] Illekova E, Svec P, Miglierini M. J. Non-Cryst. Solids, 353 (2007) 3342.

[21] Illekova E, Gachon J.C, Rogachev A, Grigoryan H, Schuster J.C, Nosyrev A, Tsygankov P. Thermochim. Acta, 469 (2008) 77.

[22] Schuster J.C, Palm M. J. Phase Equilibria and Diffusion, 27 (2006) 255.

[23] Mida R, Kasahara M, Watanabe D. Jpn. J. Appl. Phys., 19 (1980) 707.

[24] Pearson W. B. A Handbook of Lattice Spacings and Structures of Metals and Alloys, (Pergamon Press, Oxford, 1964) p. 106.

[25] Davenport J.W, Waston R.E, Weinert M. PRB 37 (1988) 9985.

[26] Alberty R. A. Pure Appl. Chem., 8 (1973) 1349.

[27] Lewis G.N, Randall M. Revised by Pitzer, Kenneth S. & Brewer, Leo (1961). Thermodynamics (2nd ed.). New York: McGraw-Hill Book.

Chapter 8
Summary and General Conclusions

In chapter-1, a general introduction about Al-based alloys containing aluminides, their properties and their applications are presented. A special attention is given to the alloys containing platelet-like aluminide particles such as Al-Al_3Ti and Al-Al_3Zr systems. The recent advanced processing methods of these alloys are described. As advanced processing techniques, severe plastic deformation (SPD) by equal channel angular pressing (ECAP) and functionally graded materials (FGMs) by centrifugal method (CM) are explained.

In chapter-2, the effect of processing Al-5 mass% Zr alloy by ECAP on its anisotropic mechanical properties is investigated. The ECAP process was performed using routes A and B_C up to 8 passes. ECAPed samples showed a notable decrease in the size of the Al_3Zr platelets and an increased tendency to align parallel to the deformation axis with increasing the number of passes. Some anisotropy in compression strength was observed at 4 passes of deformation; however, this anisotropy became negligible after 8 passes of ECAP. The wear tests showed that the ECAPed samples have almost isotropic wear property.

In chapter-3, Al-Al_3Ti composite was processed by ECAP using routes A and B_C up to 8 passes of deformation. It is observed that, increasing the number of ECAP passes causes fragmentation of Al_3Ti platelet particles and decreases their sizes compared to their original sizes in the undeformed Al-Al_3Ti specimens. Moreover, the microstructure of route A-ECAPed Al-Al_3Ti composite samples showed a strong alignment of the fragmented Al_3Ti particles parallel to the pressing axis. On the other hand, ECAPed Al-Al_3Ti alloy specimens by route B_C have a relatively homogeneous distribution of Al_3Ti particles. In spite of this observed anisotropic microstructure of route A-ECAPed samples, all the ECAPed specimens showed small anisotropy in its wear property regardless of the applied ECAP route.

In chapter-4, Al-Al_3Zr FGMs were fabricated by the centrifugal solid-particle method (CSPM) under applied centrifugal force of 30, 60 and 120*G*. Microstructural observation along the centrifugal force direction showed that Al_3Zr platelet particles are almost oriented normal to

the applied centrifugal force direction. Volume fraction of Al_3Zr particles increases close to the ring surface. Moreover, this distribution range of Al_3Zr particles becomes broader with decreasing the applied centrifugal force. The wear anisotropy of the fabricated Al-Al_3Zr FGMs was strongly influenced by the platelet particles orientation at the test position. Investigating both of the worn surface morphology and the sub-worn surface layer showed that plastic deformation induced by wear is the dominant mechanism during the wear process of Al-Al_3Zr FGM samples. Therefore, some of the tested samples were severely deformed and an Al_3Zr particles–free layer containing Al-Zr supersaturated solid solution was observed very near to the worn surface during the wear test.

In chapter-5, the phenomenon of wear induced layer observed in chapter 4 is further investigated. Al-Al_3Ti FGMs were fabricated by the CSPM under applied centrifugal force of G= 80. The Al-Al_3Ti FGMs showed different microstructure when tested at high speeds and/or high sliding distances. The Al_3Ti particles in these FGMs were strongly sheared and Al-Ti supersaturated solid solution with free Al_3Ti particles was found in the sub-worn surface layer. The thickness of this deformed layer increased with increasing the sliding speed and/or the sliding distance. The formation mechanism of this layer was discussed in the scope of the obtained results.

In chapter-6, the effect of processing temperature on the microstructure and mechanical properties of Al-Al_3Ti FGMs fabricated by CSPM and centrifugal *in-situ* method (CISM) are evaluated. CISM-FGM showed a slower compositional gradient and larger Al_3Ti particle size than that of CSPM-FGMs. The higher temperature in the CISM-FGM resulted in higher degree of Al_3Ti platelets orientation in the outer surface of the samples compared to those of CSPM-FGM. Al-Al_3Ti FGMs prepared by the two methods presented gradual hardness distribution from the outer to the inner surface of the sample. CSPM-FGMs showed better wear resistance than the CISM-FGMs. Al-Al_3Ti FGMs fabricated by the two methods have anisotropic wear property which depends on the platelets orientation and their volume fraction at the tested position.

In chapter-7, Al-Ti system FGMs were fabricated by a novel reaction centrifugal mixed-powder method (RCMPM) under different temperatures. Effect of RCMPM processing

temperature on the formation of the intermetallic particles, their morphology and their distribution in the fabricated FGMs is investigated. Fine granular Al_3Ti were observed at relatively lower processing temperature while the known coarse platelet-like particles of Al_3Ti could be achieved at higher casting temperatures. Moreover, Ti_3Al intermetallics compound and unreacted Ti phases are found for the sample fabricated at lower processing temperature. In addition, distribution of Al_3Ti intermetallics size and their volume fraction showed a significant change when the FGMs processed at different temperatures relative to the liquidus temperature of the master alloy.

In summary, the process to be applied on Al-based alloys containing platelet intermetallics should be carefully selected. If the application requires considerably homogeneous structures with finely dispersed reinforcements, then SPD is the recommended choice. On the other hand, if the processed part will be used for tribological applications where the wear resistant surface is the essential demand, CM is the suitable method.

List of Publications

Journal Articles:

1. Shimaa El-Hadad, Hisashi Sato and Yoshimi Watanabe "Investigation of Wear Induced Plastic Deformation in Al-Al_3Ti Functionally Graded Materials Fabricated by Centrifugal Solid-Particle Method", submitted to *Scripta materialia.*
2. Shimaa El-Hadad, Hisashi Sato and Yoshimi Watanabe, Investigation of Wear Anisotropy in Severely Plastically Deformed Al/Al_3Ti Composites", submitted to *Applied Physics A.*
3. Shimaa El-Hadad, Hisashi Sato, Eri Miura-Fujiwara and Yoshimi Watanabe "Fabrication of Al- Al_3Ti/Ti_3Al Functionally Graded Materials Under a Centrifugal Force", *Materials*, **3** (2010) 4639-4656.
4. Shimaa El-Hadad, Hisashi Sato, Eri Miura-Fujiwara and Yoshimi Watanabe, "Effect of Centrifugal Casting Processing Temperature on Intermetallics Characteristics in Al/Al_3Ti Functionally Graded Materials", *Japanese Journal of Applied Physics*, No. 1 (2011).
5. Shimaa El-Hadad, Hisashi Sato, Yoshimi Watanabe, "Wear of Al/Al_3Zr Functionally-Graded Materials Fabricated by Centrifugal Solid-Particle Method " *Journal of Materials Processing Technology,* 210 (2010) 2245-2251.
6. Shimaa El-Hadad, Hisashi Sato and Yoshimi Watanabe, "Anisotropic Mechanical Properties of ECAPed Al-5%Zr Containing Platelet Particles", *Materials Science and Engineering A,* 527(2010) 4674–4679.
7. Shimaa El-Hadad, Hisashi Sato, Yoshimi Watanabe "Investigation of the Mechanical Properties in Al/Al_3Zr FGMs Fabricated by Centrifugal Casting Method", *Materials Science Forum,* 631-632 (2010) 379-384.
8. Shimaa El-Hadad, Hisashi Sato, P.D. Sequeira, Yoshimi Watanabe, Yoshihiro Oya-Seimiya, "Effects of the Processing Temperature of Centrifugal Casting on the Mechanical Properties of Al-Al_3Ti FGMs", *Materials Science Forum,* 631-632 (2010) 373-378.

9. Hisashi Sato, Shimaa El-Hadad, Oleg Sitdikov, and Yoshimi Watanabe, "Effects of Processing Routes on Wear Property of Al-Al_3Ti alloys Severely Deformed by ECAP", *Materials Science Forum,* Published, 584-586 (2008) 971-976.

Conference Presentations:

1. Shimaa El-Hadad, Hisashi Sato and Yoshimi Watanabe "Wear Induced Plastic Deformation in Al-Al_3Ti Functionally Graded Materials Fabricated by Centrifugal Solid-Particle Method", to be presented in the *International conference of Processing, Performance and Failure Analysis of Engineering Materials*, 2011, Luxor, Egypt.
2. Shimaa El-Hadad, Hisashi Sato and Yoshimi Watanabe, Investigation of Wear Anisotropy in Severely Plastically Deformed Al/Al_3Ti Composites", to be presented in the *International conference of Processing, Performance and Failure Analysis of Engineering Materials*, 2011, Luxor, Egypt.
3. Shimaa El-Hadad, Hisashi Sato, Eri Miura-Fujiwara and Yoshimi Watanabe, "Effect of Centrifugal Casting Processing Temperature on Intermetallics Characteristics in Al/Al_3Ti Functionally Graded Materials", *2nd International Symposium on Advanced Plasma Science and its Applications for Nitrides and Nano materials*, ISPlasma 2010.
4. Shimaa El-Hadad, Hisashi Sato, Yoshimi Watanabe, *The 10th International Symposium on Multiscale, Multifunctional and Functionally Graded Materials,* FGM 2008, September 22-25, Sendai, JAPAN.
5. Shimaa El-Hadad, Hisashi Sato, P.D. Sequeira, Yoshimi Watanabe and Yoshihiro Oya-Seimiya, *The 10th International Symposium on Multiscale, Multifunctional and Functionally Graded Materials,* FGM 2008, September 22-25, Sendai, JAPAN.
6. Hisashi Sato, Shimaa Elhadad, Oleg Sitdikov, and Yoshimi Watanabe, " Effects of Processing Routes on Wear Property of Al-Al_3Ti alloys severely deformed by ECAP", *The 4th International Conference on Nanomaterials by Severe Plastic Deformation*, nano SPD4, August (2008).